ANUBIS detector and its sensitivity to neutral long-lived particles

Thomas Adolphus,[20] Giulio Aielli,[18] Jahanzeb Akhtar,[8,20] Arun Atwal,[20] Martin Bauer,[5] Rachel Bentham,[13,20] Oleg Brandt,[1] Jude Burling,[20] Jon Burr,[20] Patrick Collins,[20] Louie Dartmoor Corpe,[3] Matthew Coxon,[20] Jonas Dej,[1] Sofie Nordahl Erner,[23] Cayetano Fernandez Ruiz,[1] Jindrich Jelinek,[4,7,20] Oliver Kortner,[17] Hubert Kroha,[17] Lawrence Lee, Jr.,[19,22] Christopher Lester,[1] Yingshan Liang,[1] Kaijia Liu,[20] Anna Mullin,[1] Christian Ohm,[16] David Peng,[20] Luca Pizzimento,[9] Ludovico Pontecorvo,[2] Giorgia Proto,[17] Théo Reymermier,[12,20] Michael Revering,[1] Elisa Ritz,[21] Thomas P. Satterthwaite,[14,15,20] Aashaq Shah,[1] Sinem Simsek,[11] Daniel Soyk,[17] Tom Spencer,[8,20] Paul Swallow,[1] Balint Szepfalvi,[20] Noshin Tarannum,[7,20] Olivia Valentino,[10,20] Julian Wack,[1] Yanglin Wan,[6,20] Peng Wang,[20] Esperanza Winter Lopez,[20] Monami Yoshioka,[20] and Yingchang Zhang[1]

(ANUBIS Collaboration)[*]

[1]*Cavendish Laboratory, University of Cambridge, Cambridge, United Kingdom*
[2]*CERN, Geneva, Switzerland*
[3]*Université Clermont Auvergne/Laboratoire de Physique de Clermont Auvergne, CNRS/IN2P3, France*
[4]*Institute of Experimental and Applied Physics, CTU in Prague, Czech Republic*
[5]*IPPP, Department of Physics, Durham University, Durham, United Kingdom*
[6]*School of Physics and Astronomy, University of Edinburgh, Edinburgh, United Kingdom*
[7]*Department of Nuclear and Particle Physics, University of Geneva, Geneva, Switzerland*
[8]*School of Sciences and Engineering, Glasgow Caledonian University, Glasgow, United Kingdom*
[9]*Department of Physics, University of Hong Kong, Hong Kong SAR, China*
[10]*Imperial College London, London, United Kingdom*
[11]*Istinye University, Istanbul, Turkey*
[12]*Institut de Physique des 2 Infinis (IP2I), Lyon, France*
[13]*Department of Physics and Astronomy, University of Manchester, Manchester, United Kingdom*
[14]*Department of Physics, Stanford University, Stanford, California 94305, USA*
[15]*Kavli Institute for Particle Astrophysics and Cosmology, Stanford, California 94305, USA*
[16]*KTH Royal Institute of Technology, Stockholm, Sweden*
[17]*Max Planck Institute for Physics, Munich, Germany*
[18]*University and INFN Roma Tor Vergata, Rome, Italy*
[19]*Department of Physics, University of Tennessee, Knoxville, Tennessee 37996, USA*
[20]*Formerly at: Cavendish Laboratory, University of Cambridge, Cambridge, United Kingdom*
[21]*Formerly at: Hamburg University, Hamburg, Germany*
[22]*Formerly at: Department of Physics, Harvard University, Cambridge, USA*
[23]*Formerly at: IPPP, Department of Physics, Durham University, Durham, United Kingdom*

(Received 3 December 2025; accepted 20 August 2026; published 6 November 2026)

Long-lived particles (LLPs), i.e., particles with macroscopic lifetimes $\tau > 10$ ps, appear in various extensions of the Standard Model (SM) that address fundamental questions like the particulate nature of dark matter or baryogenesis. The ANUBIS detector will achieve unprecedented sensitivity to such models compared to existing and approved experiments by instrumenting a large decay volume adjacent to the ATLAS experiment at the high-luminosity LHC with tracking detectors. This paper outlines the proposed detector layouts for ANUBIS, explores their physics potential with a scalar LLP model, and identifies the preferred layout, comparing it to other experiments. The potential background contributions are estimated using a data-driven method, and the topology of potential background events is studied using Monte Carlo simulations. Overall, the ANUBIS detector is expected to probe branching ratios down to $\mathcal{O}(10^{-6})$ for exotic decays of the Higgs boson to scalar long-lived particles with masses of 10, 15, 40, and 60 GeV and proper lifetimes of $c\tau = 2.4$, 3.0, 12, and 18 m, respectively. Moreover, for branching ratios of 0.1% of the

[*]Contact author: anubis-publications@cern.ch

Published by the American Physical Society under the terms of the Creative Commons Attribution 4.0 International license. Further distribution of this work must maintain attribution to the author(s) and the published article's title, journal citation, and DOI. Funded by SCOAP[3].

Higgs boson into long-lived scalars with a mass of 15 GeV, the ANUBIS detector can probe a $c\tau$ range between 1.1×10^{-1} m and 4.0×10^{3} m.

DOI: 10.1103/kd5j-d4fv

I. INTRODUCTION

Particles with macroscopic lifetimes $\tau > 10$ ps, also known as long-lived particles (LLPs), are a key feature of many Beyond the Standard Model (BSM) theories, including supersymmetry [1,2], hidden sector models [3,4], and exotic Higgs decays [5,6]. These particles can provide insights into problems like naturalness [2,7], dark matter [8–10], and baryogenesis [11]. Their lifetime, τ, is typically a free model parameter and hence can vary widely, from $\tau > 10$ ns and up to the Big Bang nucleosynthesis limit of $\mathcal{O}(0.1\ \text{s})$ [12]. This offers considerable flexibility for LLP candidates, making them a versatile but challenging target in the search for new physics.

Detecting LLPs, especially those that are neutral and have long lifetimes, poses significant experimental challenges. The general purpose detectors at the Large Hadron Collider (LHC) [13] such as ATLAS [14], CMS [15], or LHCb [16] are limited by their finite detection volumes, intricate backgrounds, and trigger requirements that were designed for prompt particles [17–20]. Despite a concerted experimental effort from ATLAS, CMS, and LHCb, particles with long lifetimes that decay outside the active detector volume can escape detection.

To extend the sensitivity to LLPs with longer lifetimes, several proposals for dedicated detectors have emerged. These can be roughly split into two categories that complement general purpose detectors: *forward detectors* that are positioned along the beamline and *transverse detectors* that are positioned transverse to the beamline close to an LHC interaction point. The complementarity in LLP parameter space coverage between general purpose, transverse, and forward detectors is highlighted by Physics Beyond Colliders (PBC) initiative [21] and illustrated in Fig. 1.

While forward detectors such as FASER [22] can effectively probe LLP scenarios that can be produced at small partonic center-of-mass energies, $\sqrt{\hat{s}}$, of $\mathcal{O}(1\ \text{GeV})$, their ability to search for scenarios with $\sqrt{\hat{s}} \gtrsim 10$ GeV is kinematically restricted. The same restriction also applies to beam dump experiments such as SHiP [23]. By contrast, models where the LLPs are produced at the electroweak scale of $\sqrt{\hat{s}} \approx 100$ GeV and above can be effectively probed with transverse experiments [24–29], but are kinematically inaccessible for forward experiments. Hence, transverse and forward detectors cover unique areas of LLP phase space, as shown in Fig. 1, but there is also an overlap in experimental coverage which allows for comparison between them.

This paper presents the physics case for the AN Underground Belayed In-Shaft (ANUBIS) detector, which proposes the installation of an array of tracking detectors above the ATLAS experiment at CERN [24]. By leveraging the existing infrastructure, ANUBIS aims to search for LLPs with proper lifetimes $c\tau$ ranging from $\mathcal{O}(1\ \text{m})$ to $\mathcal{O}(10^5\ \text{m})$, complementing the sensitivity of ATLAS. It offers a cost-effective means of enhancing LLP searches, by modifying the ATLAS experimental environment.

A prototype demonstrator *pro*ANUBIS consisting of one ANUBIS tracking station module was installed in 2023 close to the ceiling of the ATLAS cavern [30,31] and successfully commissioned [32]. Since then, the *pro*ANUBIS detector has recorded 104 fb^{-1} and 73 fb^{-1} of pp collision data at $\sqrt{s} = 13.6$ TeV in 2024 and 2025, respectively. The main physics goal of *pro*ANUBIS is a direct measurement of hadron interactions in a background-enriched region, which then can be used to refine the tracking and vertexing algorithms, inform detector performance benchmarks for ANUBIS, improve background simulations, and further optimizations. First *pro*ANUBIS performance results were published recently [33], and the deeper analysis of *pro*ANUBIS data is underway.

This document is structured as follows: Sec. II presents the detector geometry configurations that are considered for ANUBIS, followed by a detailed discussion of the relevant background sources predictions, an evaluation of their potential contributions, and a study of their topological signature in Sec. III. Finally, a study of the projected sensitivity to LLPs using a standard benchmark endorsed by the Physics Beyond Colliders initiative [34] of CERN is

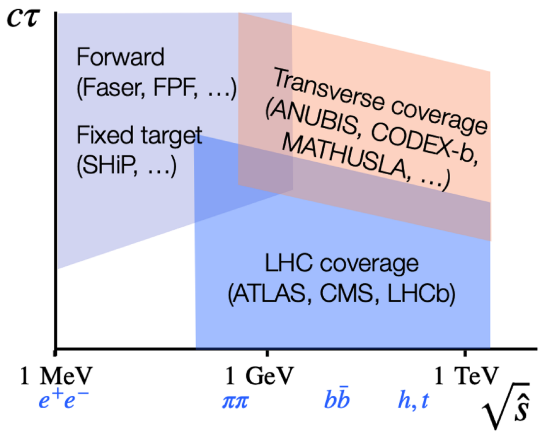


FIG. 1. Schematic representation of the coverage of different experiments to the proper lifetime $c\tau$, and partonic center-of-mass energy, $\sqrt{\hat{s}}$.

presented in Sec. IV. Based on these findings, a strong case is made for the construction of the ANUBIS detector.

II. THE ANUBIS PROJECT AND ITS LAYOUT

The ANUBIS detector exploits the "smoking gun" signature of neutral LLP decays: an isolated displaced vertex (DV) of charged particle tracks emanating from the decay position of the LLP some distance away from the interaction point. It will utilize resistive plate chambers (RPCs) as the tracking technology. A triplet of RPCs stacked on top of each other form a "tracking layer," and two tracking layers separated by ∼1 m compose a tracking station (TS) of ANUBIS [24]. Two detector configurations of the ANUBIS project, as depicted in Fig. 2, are evaluated through simulation studies.

The "shaft configuration" was the first studied and involves suspending four tracking stations within the ATLAS PX14 service shaft, at distances ranging from 23 to 80 meters from the beamline. This corresponds to the layout in the original ANUBIS proposal [24]. However, this geometry is subject to operational complications that became apparent in discussions with the ATLAS technical coordination team [35]. For example, the TSs of ANUBIS would require removal during periods such as a year-end technical stop (YETS) when the service shafts are required for crane access to the ATLAS experimental cavern, UX15. While this does not represent an insurmountable challenge, it is considered impractical given the time required to extract four TSs and the limitations on space in the SX15 hall above the PX14 service shaft that is needed for the disassembly of the TSs for further transport and storage during the YETS. Moreover, the Point 1 experimental site of the ATLAS detector does not provide sufficient space to host four TSs, which would require an involved transport to the Meyrin site, where space is also limited. Besides these two points, the discussions with the ATLAS technical coordination team and with CERN civil engineering experts did not highlight any other critical points for the installation of the ANUBIS detector.

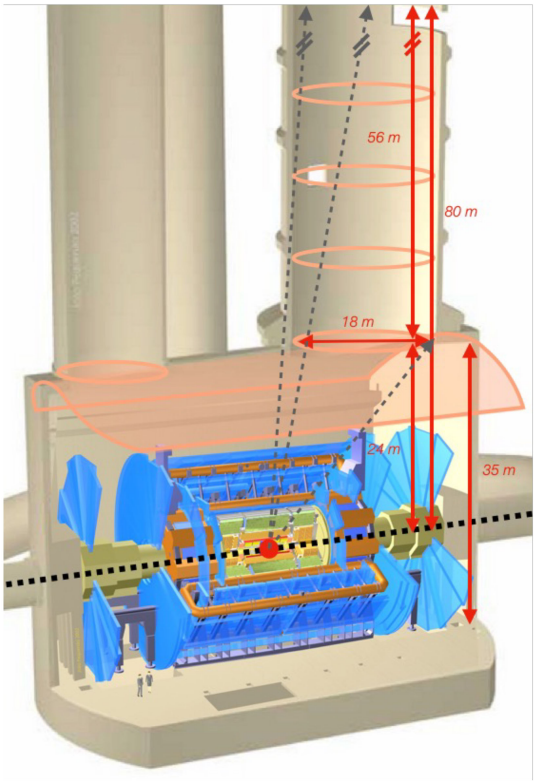


FIG. 2. Layout of the underground cavern at LHC Point 1, UX15, featuring the ATLAS experiment and the PX14 and PX16 service shafts above it. The two proposed configurations of the ANUBIS detector are shown in orange, where the shaded area illustrates the potential ceiling configuration. This includes two circular stations at the bottom of the two access shafts. The shaft configuration is indicated by the four circular stations within the PX14 service shaft, and has a solid orange line.

The other configuration considered is the "ceiling configuration" where two tracking layers separated by 1 m are installed directly onto the ceiling of the ATLAS cavern, approximately 23 m above the beamline, alongside two circular stations that are positioned at the bottom of the PX14 and PX16 service shafts. As in the original "shaft configuration," these two TSs at the bottom of the two service shafts would also need to be removed when they are required by ATLAS. These TSs can be extracted as several parts rather than a full circular station, but having only one TS per shaft will reduce the space requirement in the limited temporary storage/disassembly location immediately next to the shaft in the SX1 hall above the UX15 ATLAS cavern, and on the mid-term storage for the TSs during YETS. Moreover, this configuration would have a larger solid angle coverage than the shaft configuration, offering a broader detection range, making it highly effective for capturing LLP decays that fall between the ATLAS vertex detector's limits and the cavern ceiling, but this also leads to a smaller decay length acceptance. Hence, the ceiling configuration is considered the default in the following.

It is foreseen to fully integrate ANUBIS with ATLAS, which will enable ANUBIS to initiate trigger signals for ATLAS and vice versa. Technically, this is possible given that the ATLAS Level 0 trigger at the High-Luminosity LHC (HL-LHC) will operate with a latency window of not less than 5.5 μs [36], while ANUBIS's latency is expected to be less than 3 μs. This is mostly due to the signal propagation time and the data acquisition electronics. Both tracking and vertexing are computationally straightforward since the stray magnetic field of ATLAS should not affect the trajectories of charged particles outside of ATLAS significantly [37]. The full integration with ATLAS will benefit ANUBIS in several ways:

(i) First and foremost, the full record of a pp collision with a DV from a candidate LLP event is essential

for reducing background contributions, as will be discussed in Sec. III. For example, a true DV detected by ANUBIS is likely to coincide azimuthally with significant missing transverse momentum (E_T^{miss}) measured by ATLAS.[1]

(ii) Second, a *continuous* active decay volume would be established between ATLAS and ANUBIS, extending from the interaction point to approximately the ceiling of the ATLAS cavern. This maximizes the combined sensitivity of ATLAS and ANUBIS to LLP scenarios with decay lengths L ranging from a few μm to tens of meters.

(iii) Third, the full integration allows ATLAS and ANUBIS to probe scenarios where LLPs are produced in association with prompt SM particles like e.g., W or Z bosons in scenarios with heavy neutral leptons [38–40] or models with exotic Higgs decays into axions such as $h \to Za$ that could provide unique information on the UV completion of the axion theory [41,42]. These are expected to have negligible background contributions.

III. BACKGROUNDS

After reviewing potential sources of backgrounds for the ANUBIS detector in Sec. III A, Section III B discusses the reduction of these backgrounds by leveraging the passive shielding effect of the ATLAS detector and the information about the prompt part of the pp collision event recorded by the ATLAS detector. This strategy provides an almost background-free experimental environment for LLP searches with the ANUBIS detector, as demonstrated using a data-driven method in Sec. III C. The experimental signature of hadronic interactions that represent the dominant background contribution is studied using simulations in Sec. III D.

A. Background sources

Several types of background sources can potentially contribute to LLP detectors like ANUBIS:

(i) cosmic rays;
(ii) beam-induced backgrounds like beam-gas and beam-collimator interactions;
(iii) backgrounds from decays of quasi-thermal neutrons;
(iv) random coincidences of unrelated tracks;
(v) from SM particles with macroscopic lifetimes, subsequently referred to as "SM LLPs".

The first three background sources are evenly distributed in time and can be effectively rejected using the excellent timing resolution of ANUBIS or the event topology, as discussed in the original ANUBIS proposal [24]. The background from random coincidences of unrelated tracks is inversely proportional to the distance from the interaction point and is negligible for $L \gtrsim 1$ m, which is also discussed in Ref. [24].

The dominant potential background contribution to ANUBIS is from SM LLPs. There are only two electrically neutral SM LLPs that are relevant for ANUBIS given its large active decay volume several metres away from the interaction point: long-lived neutral kaons, K_L^0, and neutrons, n. These are characterized by mean proper lifetimes of $c\tau = 15.3$ m and 2.7×10^{11} m, respectively [43]. SM LLPs can contribute via two principal mechanisms: decays into charged particles that are registered as a DV, and the production of hadrons in collisions with material, which shall be referred to as "hadronic interactions."

Decays of K_L^0 produce at most two charged particle tracks with the exception of a few rare decay modes. Of these the dominant decay, $K_L^0 \to \pi^{\pm} e^{\mp} \nu e^{+} e^{-}$, contributes a branching ratio of 1.26×10^{-5} [43]. The tracks from K_L^0 decays are highly collimated given its typical boost factor $\gamma \gtrsim 20$. Hence, the resulting DVs have a small opening angle of $\mathcal{O}(1°)$, which makes them easy to separate from a potential LLP signal that is typically characterized by larger opening angles due to their larger mass and hence smaller boost. Furthermore, only a small fraction of K_L^0 that escape the ATLAS detector decay inside the ANUBIS active volume because of their large γ factor. The n decays, given their long lifetime, contribute negligibly inside the ANUBIS active decay volume, leaving hadronic interactions as the primary mechanism for n to contribute background to ANUBIS.

Hadronic interactions are the dominant background mechanism from SM LLPs in ANUBIS. They typically produce a handful of charged hadrons that are registered as a DV with a sizeable opening angle, see Sec. III D. Hence, the signature of hadronic interactions can be similar to that from LLP decays. One of the key advantages of ANUBIS is its *air-filled* active decay volume, this dramatically reduces the background from hadronic interactions, which are linearly proportional to the nuclear density of material traversed by the SM LLP. More precisely, the air-filled active decay volume of ANUBIS reduces the likelihood of a hadronic interaction by a factor of $\mathcal{O}(10^4)$ relative to the tile hadronic calorimeter of ATLAS. This can be understood by comparing the nuclear interaction length for air of $\Lambda_{I,\text{Air}} = 7.5 \times 10^4$ cm to that of the tile calorimeter $\Lambda_{I,\text{Tile}} = 30.3$ cm, steel $\Lambda_{I,\text{Fe}} = 16.8$ cm, and aluminium support structures $\Lambda_{I,\text{Al}} = 39.7$ cm [43].

[1]ANUBIS adopts the right-handed coordinate system of ATLAS, where its origin is at the nominal interaction point in the center of the ATLAS detector and the z axis points along the beam pipe. The x axis points from the Interaction Point (IP) to the center of the LHC ring, and the y axis points upward. Polar coordinates (r, ϕ) are used in the transverse plane, ϕ being the azimuthal angle around the z axis. The pseudorapidity is defined in terms of the polar angle θ as $\eta \equiv -\ln\tan(\theta/2)$ and is equal to the rapidity $y = \frac{1}{2}\ln(\frac{E+p_z}{E-p_z})$ in the relativistic limit. Angular distance is measured in units of $\Delta R \equiv \sqrt{\Delta\eta^2 + \Delta\phi^2}$.

B. Background reduction using ATLAS

The potential background contribution from SM LLPs is substantially attenuated by $\mathcal{O}(10^5)$ by the ATLAS detector acting as passive shielding. The calorimeters alone account for 9.7 Λ_I at $\eta = 0$ [14], resulting in an attenuation factor of 6.1×10^{-5}. Also taking into account the support structures, the solenoid, and other material upstream of the calorimeters provides a total shielding equivalent to 11.2 Λ_I at $\eta = 0$ and increasing to 13.1 Λ_I at $|\eta| = 0.7$ [14]. The flux of SM LLPs emanating from the interaction point is then reduced to 1.4×10^{-5} and 2.0×10^{-6} of its original value, respectively.

While the attenuation of the SM LLP flux emanating from the interaction point by the ATLAS detector material is quite substantial, the surviving flux of K_L^0 and n remains considerable at the HL-LHC given the total inelastic cross section of about 80 mb [44–46], which is dominated by QCD multijet processes. This source of potential background can be further reduced using topological and kinematic selections on the prompt part of the pp collision event registered by the ATLAS detector, i.e., using the ATLAS detector as an *active veto* as outlined in the original ANUBIS proposal [24]. In the first tier of the active veto, a selection on the missing transverse momentum reconstructed by the ATLAS experiment of $E_T^{\text{miss}} > 30$ GeV is applied. This requires that the SM LLPs that escape detection by the ATLAS calorimeter, and hence could initiate a hadronic interaction inside ANUBIS's active volume, be quite energetic, carrying a transverse momentum of $p_T \gtrsim 30$ GeV. Subsequent active veto selections exploit the fact that SM hadrons, including K_L^0 and n, tend to be produced in association with other hadrons that are reconstructed as jets. In particular, events with candidate LLP DVs in close angular proximity $\Delta R \equiv \sqrt{\Delta\eta^2 + \Delta\phi^2}$ to energetic prompt jets with $p_T > 15$ GeV reconstructed by the ATLAS detector are vetoed if $\Delta R(\text{DV}, \text{jet}) < 0.5$. In the same way, a similar veto is applied considering prompt charged particle tracks with $p_T > 5$ GeV if $\Delta R(\text{DV}, \text{track}) < 0.5$. The latter angular isolation requirement aims to eliminate background contributions from SM LLPs inside jets with few high-momentum particles.

The active veto using the information from the ATLAS detector reduces the potential background contribution from SM LLPs by several orders of magnitude. In addition to reducing the SM LLP flux from the interaction point, the angular isolation requirements on the DV are essential to remove any background contributions from nonprompt K_L^0 or n production in hadronic showers that are initiated in the ATLAS calorimeters, since these showers would be registered by the calorimeter and reconstructed as jets.

C. Background predictions for ANUBIS

The dominant hadronic interaction backgrounds at ANUBIS are challenging to model using Monte Carlo (MC) simulations at the required precision level. Hence, a data-driven approach is used to estimate the background contributions.

The background estimate follows the strategy of the original ANUBIS proposal [24] and is based on a search for LLPs with decay lengths of $\mathcal{O}(3\text{ m})$ using 36 fb^{-1} of pp collisions at $\sqrt{s} = 13$ TeV recorded by the ATLAS detector [20]. The search identifies LLP candidates through DVs reconstructed in the ATLAS muon spectrometer (MS), which makes it very similar to ANUBIS in terms of detector technology, analysis strategy, targeted models, and $\sqrt{s}$. In fact, this ATLAS search inspired the active veto selection outlined in Sec. III B. The background estimate for ANUBIS follows the DV + E_T^{miss} analysis strategy in the barrel region, defined by $|\eta| < 0.7$, which is most similar to ANUBIS in terms of kinematics, backgrounds, and instrumentation. This ATLAS search observed $N_{\text{bgr,ATLAS}} = 224$ events, which is consistent with the data-driven background estimate of $243 \pm 38\,(\text{stat}) \pm 29\,(\text{syst})$ obtained using uncorrelated sidebands, also known as the ABCD method [20].

The ANUBIS background estimate is obtained by scaling $N_{\text{bgr,ATLAS}}$ to the conditions expected for ANUBIS,

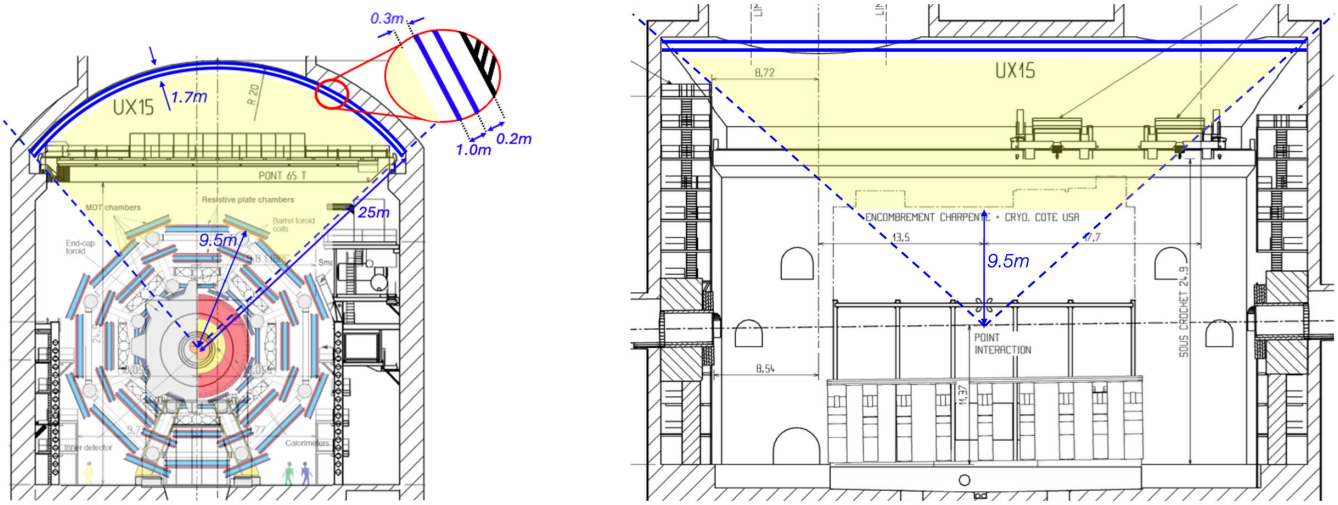
$$N_{\text{bgr,ANUBIS}} = \frac{\mathcal{L}}{\mathcal{L}'} \times \frac{\Lambda_{I,\text{MS}}}{\Lambda_{I,\text{Air}}} \times \frac{\varepsilon}{\varepsilon'} \times \frac{L_{\text{eff}}}{L'_{\text{eff}}} \times f_{\text{bgr,MS}} \times N_{\text{bgr,ATLAS}}, \tag{1}$$

where $\mathcal{L}$ is the integrated luminosity, ε denotes the reconstruction efficiency, Λ_I represents the nuclear interaction length of a given region, $f_{\text{bgr,MS}}$ is the fraction of ATLAS backgrounds produced in the MS, and primed quantities refer to ATLAS and the nonprimed ones to ANUBIS. Equation (1) captures the differences in the active detector volume, V, through the effective path length $L_{\text{eff}} \equiv \int_V \text{d}\Omega\text{d}\ell$, i.e., the integral over the solid angle, Ω, and the path, ℓ, where the path element, $\text{d}\ell$, points away from the interaction point, since the angular flux of SM LLPs $\frac{\text{d}^2N}{\text{d}\Omega dt}$ is constant as a function of distance in the absence of scattering. This conservative definition of L_{eff} ignores the decrease of the SM LLP flux with ℓ as it is depleted by hadronic interactions.

The effective path length for ATLAS is calculated following Ref. [24] as,

$$L'_{\text{eff}} = \int_0^{2\pi} \int_{0.92}^{2.22} \int_{R_{\text{in}=4.3\text{ m}}}^{R_{\text{out}=7\text{ m}}} \text{d}\phi\text{d}\theta \sin\theta \text{d}\ell = 22.1\text{ m}, \tag{2}$$

where the θ boundaries are defined by $\eta = \pm 0.7$ and the path element $\text{d}\ell$ is conservatively bounded by the region between the innermost layer of the MS and the outermost radius before the DV reconstruction efficiency significantly drops [47].



(a) (b)

FIG. 3. Two layers of the tracking stations of the ANUBIS detector for the ceiling configuration are shown inside the UX15 cavern including the ATLAS detector in (a) the (x, y) plane and (b) the (y, z) plane. The active volume is indicated as a shaded yellow region and the acceptance boundaries in η and ϕ are highlighted as dashed blue lines. The drawings of the ATLAS detector and the cavern courtesy of ATLAS.

For ANUBIS in the ceiling configuration, the effective path length is similarly calculated as,

$$L_{\text{eff}} = \int_V \frac{1}{|\vec{r}|^2} \mathrm{d}^3\vec{r} = 32.3 \text{ m}. \tag{3}$$

Here, V is bounded toward the beamline by the outer layer of the ATLAS muon spectrometer (9.5 m). The ceiling of the ATLAS cavern dome defines the V boundary away from the beamline. The cavern dome has a curvature radius of 20 m, where the beamline is displaced by 1.7 m toward the center of the LHC ring and by 3.5 m downward relative to the center of curvature. The crossing points of the ceiling dome with the walls of the ATLAS cavern define the radial V boundary through direct lines connecting them to the interaction point. A drawing of the ANUBIS detector in the ceiling configuration inside the UX15 cavern including the ATLAS detector is shown in Figure 3, where the active volume considered for the background estimate is indicated as a shaded region and the acceptance boundaries in η and ϕ are highlighted as dashed lines.

Background events from hadronic interactions in the ATLAS search include DVs produced in both the outer layers of the ATLAS calorimeter and the ATLAS MS. The reconstruction efficiency of DVs from hadronic interactions in the calorimeter displays a strong variation as a function of ℓ. This is due to a combination of decay products being stopped within the calorimeter before reaching the MS and observed deposits in the calorimeter causing the events to fail isolation requirements. By contrast, the reconstruction efficiency of DVs from hadronic interactions in the MS is relatively stable as a function of ℓ until it drops around 7 m [47]. Hence, only the events with DVs that are consistent with being produced in the MS are used for the ANUBIS background prediction. Their fraction relative to the total number of ATLAS background events is captured by $f_{\text{bgr,MS}} = 0.65$, calculated by measuring the relative longitudinal density of vertices seen in ATLAS within the calorimeter and MS and correcting for vertex migration due the finite precision of the DV reconstruction algorithm.

The average nuclear interaction length within the ATLAS MS, $\Lambda_{I,\text{MS}}$, is calculated using the average density of aluminium and iron in the MS, measured from the ATLAS geometry simulation [48]. Conservatively, any materials within the MS other than aluminium and iron are neglected, resulting in $\Lambda_{I,\text{MS}} = 385$ cm.

With the estimates of the effective path length from Eqs. (2) and (3), using a projected HL-LHC integrated luminosity of 3 ab^{-1}, and conservatively assuming that, due to their uniform coverage, the ANUBIS detectors will be two times more efficient than the current ATLAS muon system in the context of reconstructing background DVs, Eq. (1) yields,

$$\begin{aligned} &N_{\text{bgr,ANUBIS ceil.}} \\ &= 0.86 \times \frac{\int_{V=\text{ceil.}} \mathrm{d}\Omega \mathrm{d}\ell}{\int_{V'=\text{ATLAS}} \mathrm{d}\Omega \mathrm{d}\ell} \times f_{\text{bgr,MS}} \times N_{\text{bgr,ATLAS}} \\ &= 0.56 \times \frac{32.3 \text{ m}}{22.1 \text{ m}} \times N_{\text{bgr,ATLAS}} \\ &= 182.4 \pm 12.2. \end{aligned} \tag{4}$$

As a cross-check of the above technique, an alternative background prediction was made by rescaling the

interactions within the ATLAS calorimeter instead of those in the MS. In this estimate, the dependence of the DV reconstruction efficiency on the distance from the beamline was explicitly taken into account. Using the efficiencies from the ATLAS search for a range of signals, along with the relative volume of calorimeter and its average material density, the calorimeter-based estimates predict backgrounds ranging from 19 to 107 events. As the MS-based estimate produces the more conservative prediction and has a lower uncertainty due to not needing to estimate the differential vertex reconstruction efficiency, it is used as the primary background prediction. Given the conservative assumptions and taking the MS-based background estimate rather than the calorimeter-based one, these projections will be referred to as "conservative" in the following.

Recently, ATLAS has published a new search for LLPs with decay lengths of $\mathcal{O}(3\text{ m})$ using 140 fb^{-1} of pp collision data at $\sqrt{s} = 13$ TeV [41]. This new analysis is conceptually similar to the results using 36 fb^{-1} of data from Ref. [20], but achieves an even higher background rejection rate through machine learning techniques, and gives the background contribution in the barrel region as $241 \pm 18\,(\text{stat}) \pm 6\,(\text{syst})$, which is consistent with the observation of $N_{\text{bgr,ATLAS,140 fb}^{-1}} = 245$. Using this background estimate in Eq. (4) and accounting for the different ratio of integrated luminosities between the ATLAS analyses gives

$$N^{\text{from 140 fb}^{-1}}_{\text{bgr,ANUBIS ceil.}} = 51.3 \pm 3.2. \tag{5}$$

While the estimate from Eq. (5) underlines the potential sensitivity of ANUBIS to LLP signals that could be achieved using multivariate machine learning techniques, and hence supports "nominal projections", the results from Eq. (4) are considered for the "conservative" projections.

For ANUBIS in the shaft configuration, which corresponds to the "shaft+cone" scenario in the original ANUBIS proposal [24], the effective path length was calculated as $L_{\text{eff}} = 11.3$ m. This results in

$$N_{\text{bgr,ANUBIS shaft+cone}} = 63.7 \pm 4.3. \tag{6}$$

The actual number of background events in the HL-LHC dataset is likely to be lower than indicated in Eqs. (4) and (5). To provide a bound on the best-case ANUBIS sensitivity, a "background-free" projection is also provided in Sec. IV F. Hence, the actual sensitivity of ANUBIS is bracketed by the "background-free" projections and the "conservative" projections based on Eq. (4). Note that searches requiring the presence of two LLPs in the combined active volume of ANUBIS and ATLAS can safely be considered background-free. The same is true for scenarios where LLPs are produced in association with prompt energetic SM particles e.g., a W or Z boson that are required to be registered by ATLAS.

D. Signature of hadronic interactions in ANUBIS

As outlined in Sec. III A, SM LLPs represent the dominant potential source of background for ANUBIS: both K^0_L and n can contribute through hadronic interactions, while decays are only relevant for the former. Despite low background levels presented in Sec. III C, it is prudent to study in detail the topology of contributions from SM LLPs to understand what signature they will present to the ANUBIS detector.

As reported in Ref [49], a sample of minimum-bias pp collision events at $\sqrt{s} = 14$ TeV is generated using Pythia8 [50] using the MSTW2008 parton distribution functions [51] with the A2 tune [52]. Out of 10^{10} simulated collisions, approximately 2.3×10^7 n and 1.7×10^7 K^0_L particles are produced. In the next step, a separate simulation is carried out using Geant4 [53] to model n and K^0_L interactions by firing them into a coaxial air-filled cylinder of 100 m in length and 20 m in radius. In this simulation SM LLPs are generated following the three-momentum distributions in the minimum bias event sample generated in the first step.

The Geant4 simulations show that in the majority of events the SM LLP particles pass through the air-filled cylinder, which is expected given $\Lambda_{I,\text{Air}}$. In the remainder of the events, the SM LLP particles undergo a hadronic interaction, with a small fraction of K^0_L decaying. Only events with at least two charged particles in the final state are retained for further analysis, since no DV can be reconstructed otherwise. The resulting sample of events will be referred to as the "interaction sample."

The results of the Geant4 and Pythia8 simulations are combined for further analysis. For each n or K^0_L in the minimum bias sample, a corresponding particle with a three-momentum within 50 MeV of the minimum bias particle is randomly selected from the interaction sample. The resulting event is then weighted according to the probability of generating the required multiplicity of charged final-state particles, based on the fraction of events in the interaction sample within the 50 MeV momentum window that met this condition. If no kinematic match is found, the three-momentum acceptance threshold is increased in 50 MeV increments until a match is found.

The trajectories of final-state charged particles produced in the step above are subject to an angular transformation that aligns the three-momenta of the SM LLP in the interaction sample to the corresponding matched SM LLP in the minimum bias sample. Hence, the Pythia8 simulation of minimum bias events contributes the type of the SM LLP as well as its trajectory and event-level properties like E_T^{miss}, while the Geant4 simulation of the interaction sample supplies details on the distance travelled by the SM LLP before interaction with air or decay, and the spectrum of particles produced. The resulting events were subjected to the event-level selection criteria from Sec. III B: $E_T^{\text{miss}} > 30$ GeV and $\Delta R > 0.5$ between the DV and the closest reconstructed jet or charged particle.

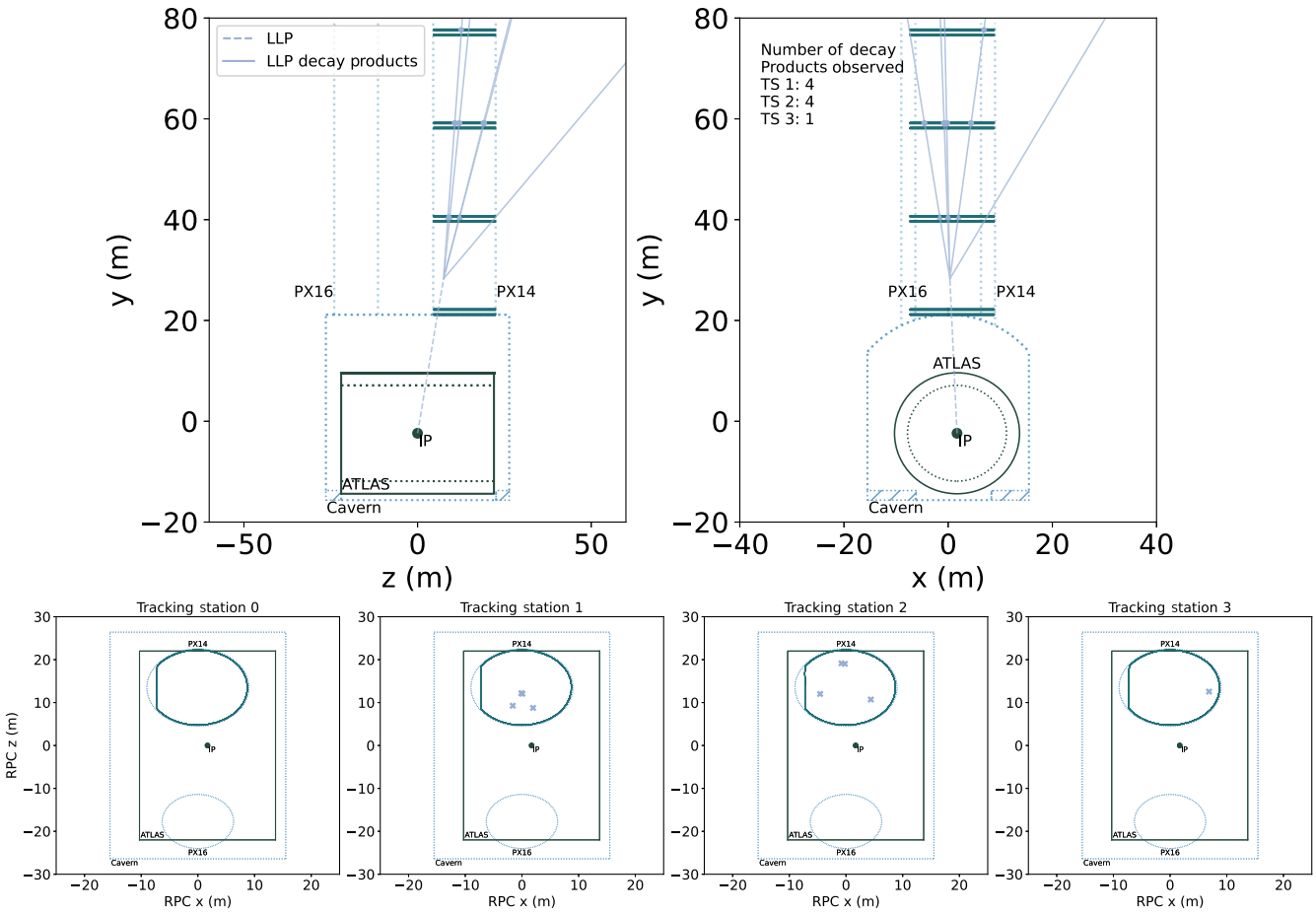


FIG. 4. Display of a representative background candidate event featuring a hadronic interaction induced by a n inside the ATLAS Cavern. Dashed lines represent the LLP trajectory, while solid lines show the trajectories of the ensuing jet of four charged final-state particles. Cross-sections of the ATLAS cavern and service shafts in the zy- (top left) and xy- (top right) planes, with dotted lines representing ATLAS' vertexing limit. The xz intersection points of the final-state, charged particles with ANUBIS's tracking stations inside the shaft (bottom) are shown as crosses.

The charged particle multiplicity in the selected background event sample originating from hadronic interactions peaks at four and shows an exponentially falling tail extending up to 20. These numbers include low-energetic secondary $e^{\pm}$ from converted Bremsstrahlung photons, $\pi^0 \to \gamma\gamma$ decays, etc. The angular distribution between the trajectories of the charged particles and the original trajectory of a SM LLP steeply increases up to an angle of about 0.2 rad and falls exponentially after that. For the K_L^0 decays, the charged particle distribution is dominated by a peak at two, and has an angular distribution peaking at 0.02 and extending up to 0.05. Hence, K_L^0 decays can be easily discriminated against using their signature of two very collimated charged particle tracks. However, the topology of potential background events from hadronic interactions can mimic the topology of the signal in principle. This underlines the pivotal advantage of the air-filled active decay volume of ANUBIS, which allows for maximal reduction of the contribution from hadronic interaction.

To study the potential impact of hadronic interactions in the context of the geometry of the ANUBIS detector, the trajectories of charged particle tracks are propagated to determine if they would intersect with the ANUBIS tracking stations. At least two charged particles are required to intersect with the tracking stations, since at least two reasonably energetic tracks are required to produce a reconstructable displaced vertex. This approach assumes the detector to be 100% efficient for charged particles. This approximation is made since a single RPC detector features a detection efficiency of $> 98\%$, which translates into $\sim$99.9% for a tracking layer that comprises a triplet of RPC detectors with a two-out-of-three hit logic.

A representative background candidate event involving a hadronic interaction of a SM LLP, in this case a n, is displayed in Fig. 4. In this event, five charged final-state particle tracks are produced inside the shaft between the first and second TS. The second and third TS register hits from four tracks, while the fourth TS observes hits from two. No track hits are registered in the ceiling tracking

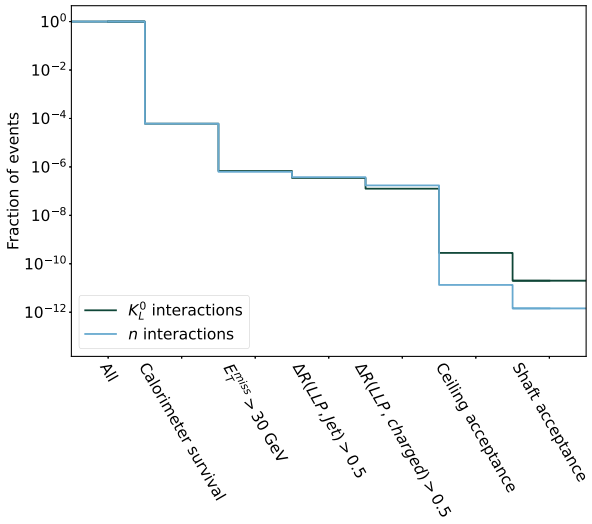


FIG. 5. Impact of successive selection requirements and background events from K_L and n interactions within the active volume of the ANUBIS detector. Note that the final two bins are noncumulative: events passing the final event-level selection are considered independently for the "ceiling" and "shaft" scenarios, respectively.

station in this particular event. The opening angle of the charged particles emanating from the DV in this example event is fairly small, as expected for hadronic interactions.

The impact of topological selections from Sec. III B on the simulated background events is studied in Fig. 5.

As expected, the shielding effect of the ATLAS calorimeters, which is conservatively[2] taken as 9.7 Λ_I [14], has the most prominent impact on the background, reducing it by 6×10^{-5}. The second most prominent selection is the $E_T^{\text{miss}} > 30$ GeV requirement, which reduces the background by another two orders of magnitude. The angular isolation requirements then reduce the background by another order of magnitude. The requirement for the SM LLP interaction to occur within the active volume of ANUBIS further reduces the background by three to four orders of magnitude, depending on the detector configuration.

Normalizing to the product of the inelastic proton-proton cross section of 78.1 mb and $\mathcal{L} = 3$ ab^{-1} [54], the above predictions are larger than the conservative data-driven estimate in Sec. III C. This disagreement is attributed to a combination of factors like the simulations not considering selections that would be performed in an actual analysis, e.g., vertex reconstruction or track or hit multiplicities, as well as potential modelling deficiencies of rare processes like hadronic interactions with air in Pythia8+Geant4 simulations.

To study these factors, a prototype demonstrator called *pro*ANUBIS consisting of one ANUBIS TS module was installed in 2023 close to the ceiling of the ATLAS cavern and has so far recorded 157.8 fb^{-1} of pp collision data [30]. One of the main physics goals of *pro*ANUBIS is the direct measurement of the expected background flux in a background-enriched region, which then can be used to refine the vertexing algorithm and other DV-related selections, background simulations, and further optimizations.

IV. SENSITIVITY STUDIES

A. Signal model

The sensitivity of ANUBIS to detect BSM neutral LLPs is evaluated through simulations of their production and decays. The primary benchmark model considered involves the Higgs boson decaying into a pair of neutral, scalar LLPs, $h \to ss$, where s denotes a new neutral scalar particle that may be long-lived. Throughout this article, s and m_s denote this scalar state and its mass, respectively.

For $m_s > 10$ GeV, each scalar is assumed to decay predominantly into a pair of b quarks, corresponding to Benchmark Case 5 (BC5) from Ref. [34]. These quarks then hadronize, producing charged particles that can be detected by the tracking layers of ANUBIS. The detection of these final-state jets provides the key signature of the signal.

The choice of exotic Higgs decays into neutral LLPs as the benchmark is motivated by their prevalence in BSM scenarios, including neutral naturalness [2,7,55] and supersymmetric models, where LLPs often arise. Furthermore, this model features a massive mediator at the electroweak scale—the Higgs boson, thereby highlighting the unique sensitivity of transverse detectors like ANUBIS and their complementarity to forward detectors. This benchmark model is endorsed by the Physics Beyond Colliders initiative for comparisons between various experiments [34] features in its ESPPU 2026 submission [21]. Signatures with displaced hadronic jets similar to BC5 presented here arise in a broad class of BSM scenarios [17].

This analysis considers the dominant Higgs boson production mechanism: gluon-gluon fusion (ggF), which accounts for 88% of Higgs production, with a cross-section of 54.67 pb at $\sqrt{s} = 14$ TeV [43]. The corresponding Feynman diagram is shown in Fig. 6.

B. Signal sample simulation

The simulated signal samples were produced using the Hidden Abelian Higgs model (HAHM) described in Refs. [3,4,56,57] to generate a ggF-produced Higgs that is forced to decay into a pair of electrically neutral scalar (s) LLPs with masses of $m_s = 10$, 20, 30, 40, 50, and 60 GeV. These were simulated using MG5_aMC@NLO 3.5.4 [58] with the NN23LO1 PDF set [59]. The produced scalar LLPs are forced to decay into a pair of b quarks with a branching ratio $\mathcal{B}r(s \to b\bar{b}) = 100\%$ via Madspin, with the subsequent hadronization and parton shower

[2]This is because the support structures are not considered here, if they are then the calorimeters should be taken as 11.2 Λ_I.

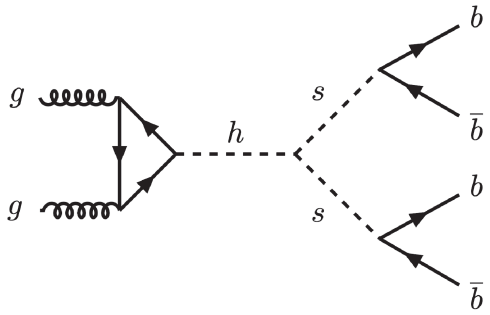


FIG. 6. Feynman diagram for the dominant scalar LLP production mechanism considered in this analysis, which is via a Higgs boson produced with gluon-gluon fusion.

simulated with the Pythia8 program. In total, approximately 4×10^6 events were simulated for each mass point. The HAHM also includes an additional dark photon, Z_d [57], which is decoupled here by setting its mass to an arbitrarily high value ($\gg m_h$) and its coupling to the Higgs boson to be zero.

C. Event selection

To identify candidate events in the signal samples consistent with neutral BSM LLP decays the selections from Sec. III B are applied: candidate LLP decays must be isolated by $\Delta R = 0.5$ from any nearby jets with $p_T > 15$ GeV and any energetic charged particles with $p_T > 5$ GeV; and $E_T^{\text{miss}} > 30$ GeV is required in the event. The E_T^{miss} selection is expected to have a moderate impact on the signal efficiency, as indicated by the p_T distribution of the Higgs boson in Fig. 7, leaving space for further tightening of the $E_T^{\text{miss}} > 30$ GeV criterion. Additionally, to better represent the response on data, a geometric acceptance cut requires the LLP decay to occur within the ANUBIS fiducial volume; and that the momentum vectors of any charged decay products of the LLP intersect with at least two RPC stations.

Figure 8 shows the impact of these selections on a signal sample with $m_s = 15$ GeV and $c\tau = 3$ m. Following the application of these selection cuts, the fraction of signal events that are retained is approximately 0.03 in the ceiling case and 0.003 in the shaft case, while the fraction of SM LLP backgrounds that are expected to survive is $\mathcal{O}(10^{-12})$ and $\mathcal{O}(10^{-11})$ for the respective geometries. This highlights the balance between signal purity and background suppression from the selection.

This selection considers a single displaced vertex (1DV) within the ANUBIS detector, however there are two scalars in the final state. Therefore, an additional constraint that there must be two displaced vertices (2DVs) in an event can be introduced, where at least one of these vertices is within the ANUBIS fiducial volume and the other is in ATLAS or ANUBIS. This requirement reduces the background level to effectively zero, since the fraction of remaining background events is $\approx 10^{-12}$ for the 1DV selection, which translates to $\approx 10^{-24}$ for the 2DVs case.

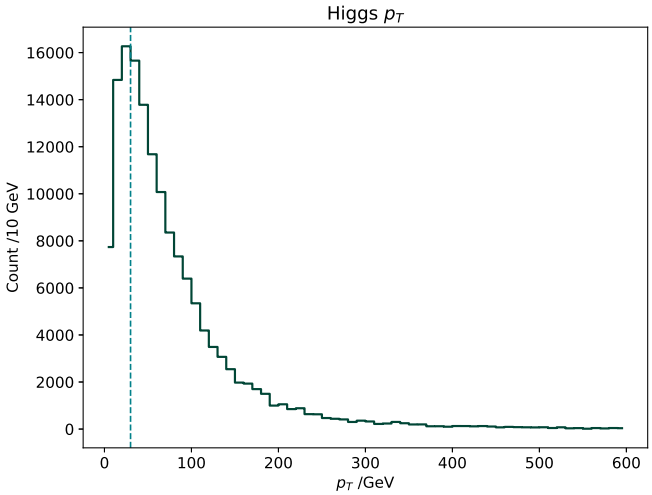


FIG. 7. Expected p_T distribution of the Higgs boson simulated for the ggF production mode. The $E_T^{\text{miss}} > 30$ GeV cut is indicated by the dashed vertical line.

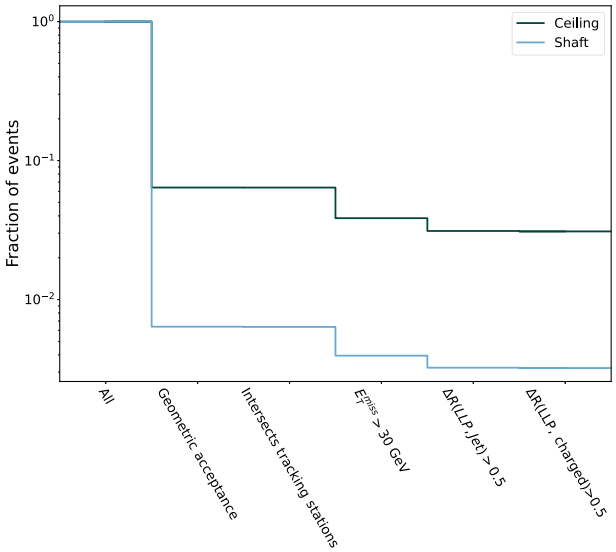


FIG. 8. Impact of successive selection requirements on the signal sample with $m_s = 15$ GeV and $c\tau = 3$ m for the ceiling and shaft ANUBIS configurations. The ordering of these cuts differs from the background case, where the geometric acceptance was performed last for the ceiling and shaft separately.

D. Detector geometry simulations

The simulation of the ANUBIS detector geometry and the corresponding acceptance for signal events is carried out following the same procedure as for background events described in Sec. III D.

For an event to be observed, the LLP must produce at least two sufficiently energetic charged particles that

intersect at least one of the ANUBIS TSs. In addition, final-state charged particles that traverse dense materials such as concrete before reaching a TS are excluded from the analysis, as they would likely be absorbed.

The decay positions of simulated LLPs are reweighted according to

$$P(x) = \frac{1}{\beta\gamma c\tau} e^{-x/(\beta\gamma c\tau)} \quad [43]. \tag{7}$$

Two configurations for the ANUBIS geometry and hence the observation of LLP decays are considered,

(i) The shaft configuration from Sec. II corresponds to the "shaft + cone" scenario from the original ANUBIS proposal. It allows the LLP to decay within the PX14 shaft or within the UX15 ATLAS experimental cavern provided the decay products traverse the lowest TS;

(ii) The ceiling scenario follows the ceiling configuration introduced in Sec. II and described in detail in Sec. III C, albeit with conservative modifications for the signal case: the active decay volume starts 9.5 m away from the beamline. This is motivated by the rapidly dropping density of material in the barrel region of ATLAS muon spectrometer at 4.5 m away from the beamline, to which 5 m are conservatively added. These additional 5 m account for the loss in the active decay volume from any material-dense regions in the ATLAS muon spectrometer like support structures or active ATLAS detector elements like RPCs or muon drift tubes, and a 30 cm safety margin around these regions on account of finite vertex resolution. It should be noted that the ATLAS vertexing limit is 7.5 m [20]. The active decay volume ends 1.5 m below the ceiling of the ATLAS cavern, which accounts for the TS (1 m), fixings and

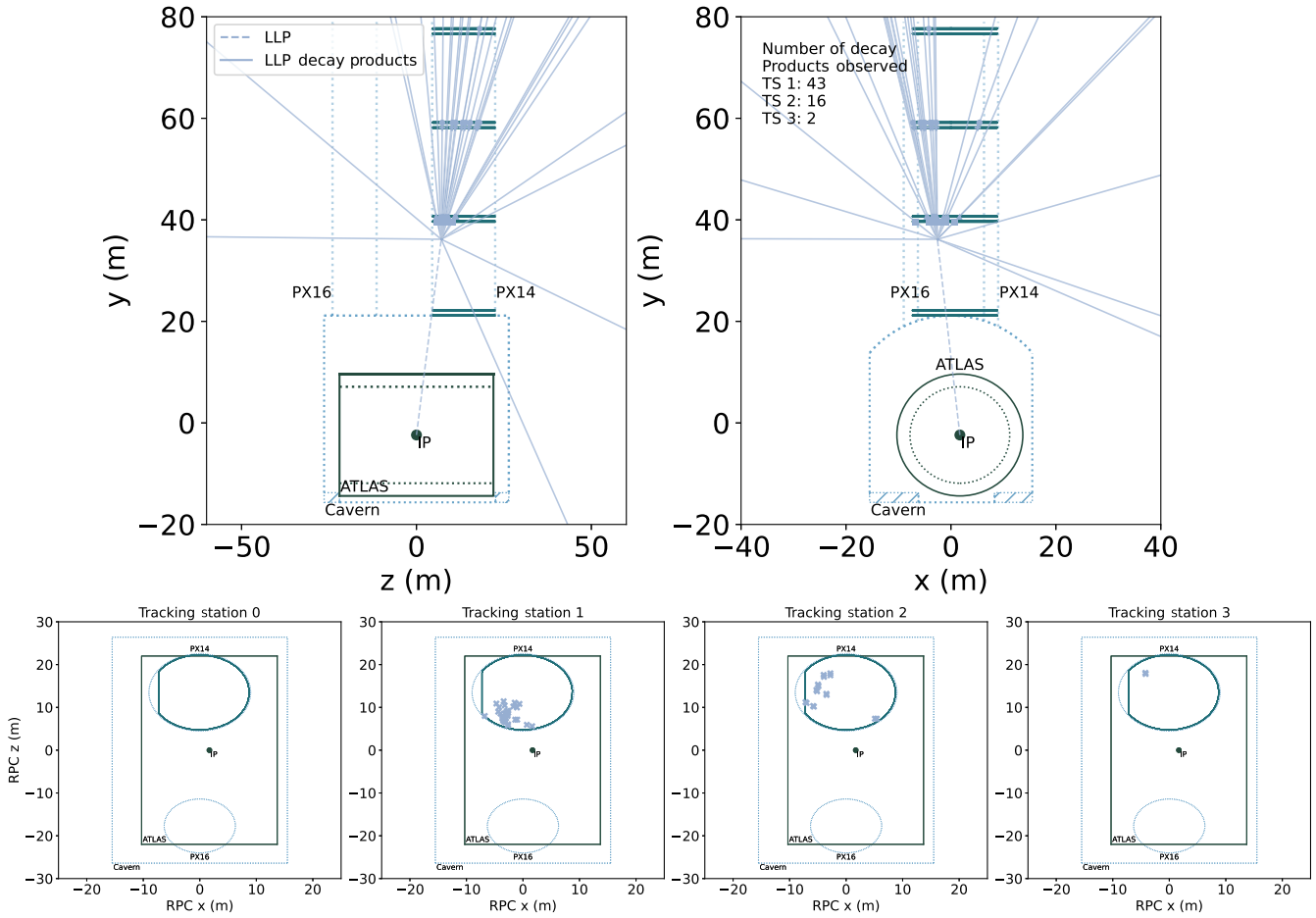


FIG. 9. Display of a representative signal event where the decay of a scalar LLP with $m_s = 15$ GeV and $c\tau = 30$ m is observed by ANUBIS in the shaft configuration after the full selection procedure. This event would not be observed in the ceiling configuration. Dashed lines represent the LLP trajectory, while solid lines show the trajectories of the ensuing charged final-state particles produced in the LLP decay. Cross-sections of the ATLAS cavern and service shafts in the zy- (top left) and xy- (top right) planes are also shown, with dotted lines representing ATLAS' vertexing limit. The intersection points of the final-state, charged particles with ANUBIS's Tracking Stations in xz projection (bottom) are shown, where each represents two triplets of RPCs separated by ∼1 m. The intersection points are represented as crosses.

services (0.2 m), and a safety margin (0.3 m) in front of the TS to ensure a reliable rejection of DVs that originate from the TS material. Hence, the radial length of the active decay volume of ANUBIS is shorter for the signal sensitivity projections than for background projections.

Representative examples of in-cavern LLP decays for the shaft and ceiling configurations are shown in Fig. 9 and Fig. 10, respectively.

In the following, it is assumed that the ATLAS magnetic field has negligible influence on the trajectory of final-state, charged particles for these configurations. This is justified since the magnetic field will have a roughly isotropic effect on the jets of energetic charged particles from LLP decays, resulting in minimal impact on overall sensitivity. In other words, the capability of measuring the transverse momenta of the charged particle tracks from LLP decays inside or close to the ATLAS muon spectrometer and hence the

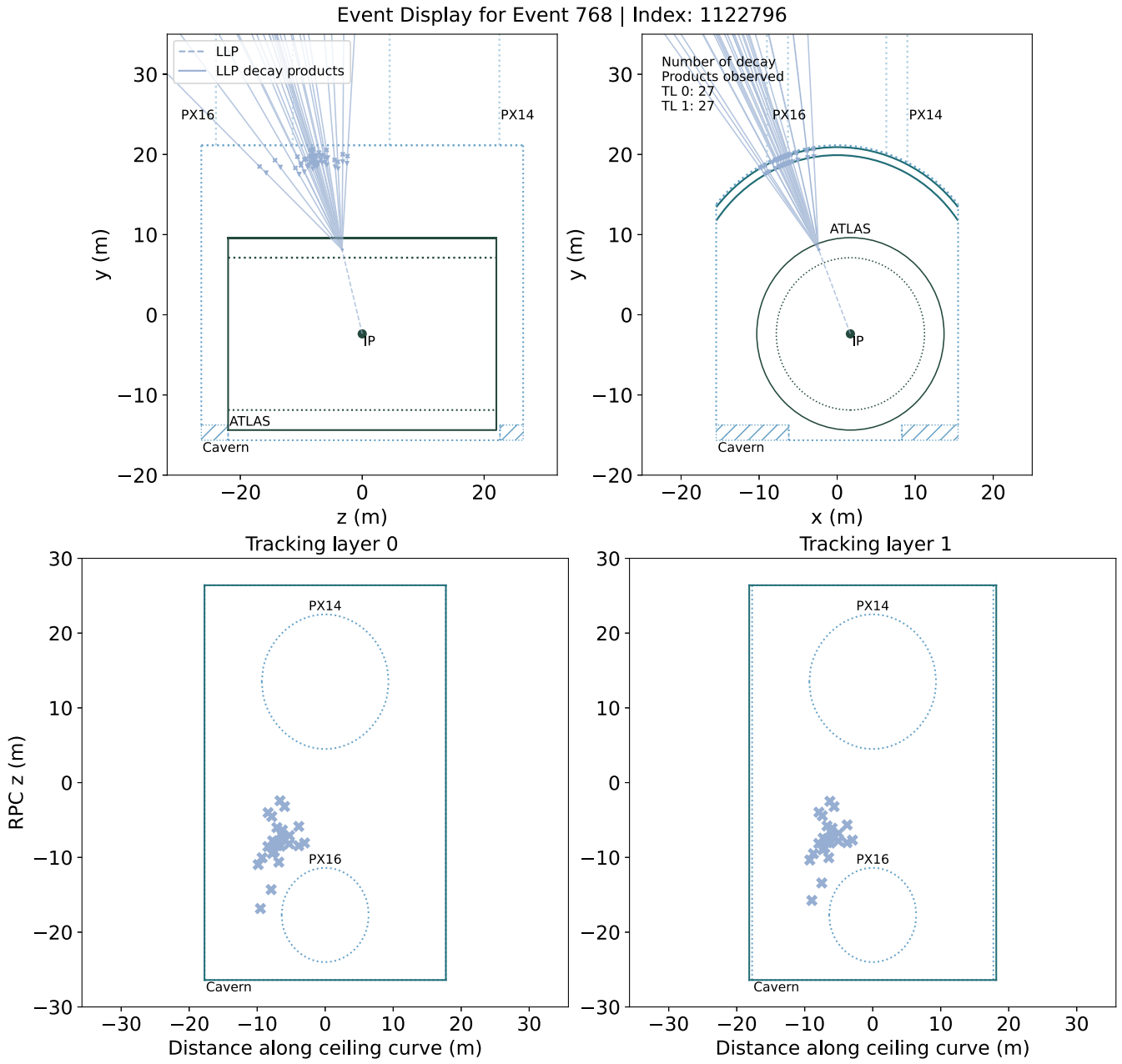


FIG. 10. Display of a representative signal event where the decay of a scalar LLP with $m_s = 15$ GeV and $c\tau = 3$ m is observed by ANUBIS in the ceiling configuration after the full selection procedure. This event would not be observed in the shaft configuration. The display follows the same format as Fig. 9, except that the intersection points of the final-state particles in both RPC triplets in the ceiling Tracking Station are shown separately as individual tracking layers. These are displayed in the local curved coordinate system of the tracking layer (bottom).

invariant mass of the DV is conservatively neglected for the sensitivity projections in Sec. IV E. However, note that this experimental capability will allow ANUBIS + ATLAS to provide a lower bound on the LLP mass from its decay into charged particles in case of a discovery.

E. Sensitivity calculation

This study probes values of $c\tau$ ranging from 10^{-3} to 10^{8} m that bound the expected sensitivity of ANUBIS, in increments of one-fifth of an order of magnitude. The geometrical and kinematic acceptance of ANUBIS, $\mathcal{A}$, is calculated by applying the selections from Sec. IV C to MC simulations from Sec. IV B, counting the number of DVs that are reconstructed in a given detector configuration outlined in Sec. IV D, and dividing by the total number of DVs produced. The hit detection efficiency is assumed to be 100% in the $\mathcal{A}$ calculation, which is a good approximation as motivated in Sec. III D. The selection efficiency for DVs from signal events ε_{sig} accounts for the efficiency of the discrimination between DVs from signal and background events considering vertex-level observables like the hit multiplicity. The ATLAS LLP search features $62\% < \varepsilon_{\text{sig}}^{\text{ATLAS}} < 74\%$ for $15 < m_s/\text{GeV} < 60$ [20]. Hence, a value of $\varepsilon_{\text{sig}}^{\text{ANUBIS}} = 50\%$ is conservatively assumed for the ANUBIS sensitivity projections, motivated by the similarity in the detector technology between ANUBIS and the barrel region of the ATLAS muon spectrometer. Note that for the background estimate in Section III C a two times higher selection efficiency was conservatively assumed for ANUBIS compared to ATLAS, despite the conservative assumption $\varepsilon_{\text{sig}}^{\text{ANUBIS}} < \varepsilon_{\text{sig}}^{\text{ATLAS}}$ above.

The number of signal events N_{sig} expected to be observable is given by

$$N_{\text{sig}} = \mathcal{L}_{\text{HL-LHC}} \cdot \sigma_h \cdot 2 \cdot \mathcal{B}r(h \to ss) \cdot \mathcal{A} \cdot \varepsilon_{\text{sig}}, \quad (8)$$

where $\mathcal{L}_{\text{HL-LHC}} = 3\ \text{ab}^{-1}$ is the integrated luminosity of pp collisions at $\sqrt{s} = 14$ TeV at the HL-LHC, $\sigma_h = 54.67$ pb [43] represents the Higgs boson ggF production cross section at $\sqrt{s} = 14$ TeV, and $\mathcal{B}r(h \to ss)$ denotes the exotic branching ratio of the 125 GeV Higgs boson into an ss pair. The factor of 2 features in Eq. (8) since a pair of LLPs are produced in the Higgs decay, either of which can potentially provide a reconstructable DV.

In practice, the expected sensitivity of ANUBIS to an exotic 125 GeV Higgs boson decay into an ss pair is calculated by solving Eq. (8) for $\mathcal{B}r(h \to ss)$ after determining $\mathcal{A}$ for a given m_s and $c\tau$ hypothesis and setting N_{sig} to the number of events required for signal observation in a given detector configuration.

Previously reported sensitivity for ANUBIS under a conservative background assumption [21,24,49,60] was given using the 5σ discovery as a figure of merit. Following the formalism from Ref. [61], this corresponds to values of $N_{\text{sig}} \geq 102$, $N_{\text{sig}} \geq 45$, and $N_{\text{sig}} \geq 52$ using Eqs. (4)–(6) for the ceiling conservative, nominal, and shaft configurations, respectively. However, for better comparison with other LLP experiments and existing experimental limits, signal thresholds were also determined for an exclusion sensitivity at the 95% confidence level (CL) using the CLs method [62]. These thresholds for the ANUBIS configurations are $N_{\text{sig}} \geq 36$, $N_{\text{sig}} \geq 17$, and $N_{\text{sig}} \geq 19$ assuming background estimates from Eqs. (4)–(6), respectively. The conservative background sensitivity projections will use the 95% CL exclusion sensitivity unless otherwise stated. The background-free sensitivity projections require $N_{\text{sig}} \geq 4$ for all detector configurations.

F. Results

Throughout this section the 1DV selection limits will be considered unless otherwise stated, as this is the most conservative scenario. Likewise, the 95% CL exclusion sensitivity will be provided.

The expected sensitivity of ANUBIS to an exotic branching ratio of the 125 GeV Higgs boson into a pair of scalar LLPs, i.e., $\mathcal{B}r(h \to ss)$, using 3 ab^{-1} of pp collisions at the HL-LHC is presented in Fig. 11 for $m_s = 10$, 15, 40, and 60 GeV for the 1DV selection. The results are shown for the two configurations of the ANUBIS detector: shaft and ceiling. Both conservative projections and background-free projections that bracket the expected sensitivity of ANUBIS are provided.

The ceiling configuration provides the best sensitivity and can probe $\mathcal{B}r(h \to ss)$ down to $\mathcal{O}(10^{-5})$ and $\mathcal{O}(10^{-6})$ for the conservative and background-free projections, respectively. It is followed by the shaft + cone configuration, where the sensitivity to $\mathcal{B}r(h \to ss)$ is reduced by about an order of magnitude in both the background-free and conservative projections. If only decays in the PX14 shaft are considered the sensitivity is further reduced by a similar amount. This sensitivity ranking is expected from the L_{eff}, which is largest for the ceiling configuration. Combined with fewer practical constraints outlined in Sec. II, this confirms the choice of the ceiling configuration as the default layout of the future ANUBIS detector.

A subtle aspect in Fig. 11 is the shift of the $c\tau$ value where the best sensitivity is achieved from $c\tau = 2.4$ m for $m_s = 10$ GeV to 18 m for $m_s = 60$ GeV considering the default ceiling configuration, which is reflected in similar trends for the other configurations. This effect is due to the increase of the boost γ with decreasing m_s.

Figure 12 compares the projected ANUBIS discovery and exclusion sensitivities in the default ceiling configuration to background-free exclusion projections from other major proposed transverse experiments at the HL-LHC: CODEX-b [63] and MATHUSLA [64]. Also shown are the exclusion limits at 95% CL from existing ATLAS [20,41] and CMS [19] searches, since no HL-LHC projections from

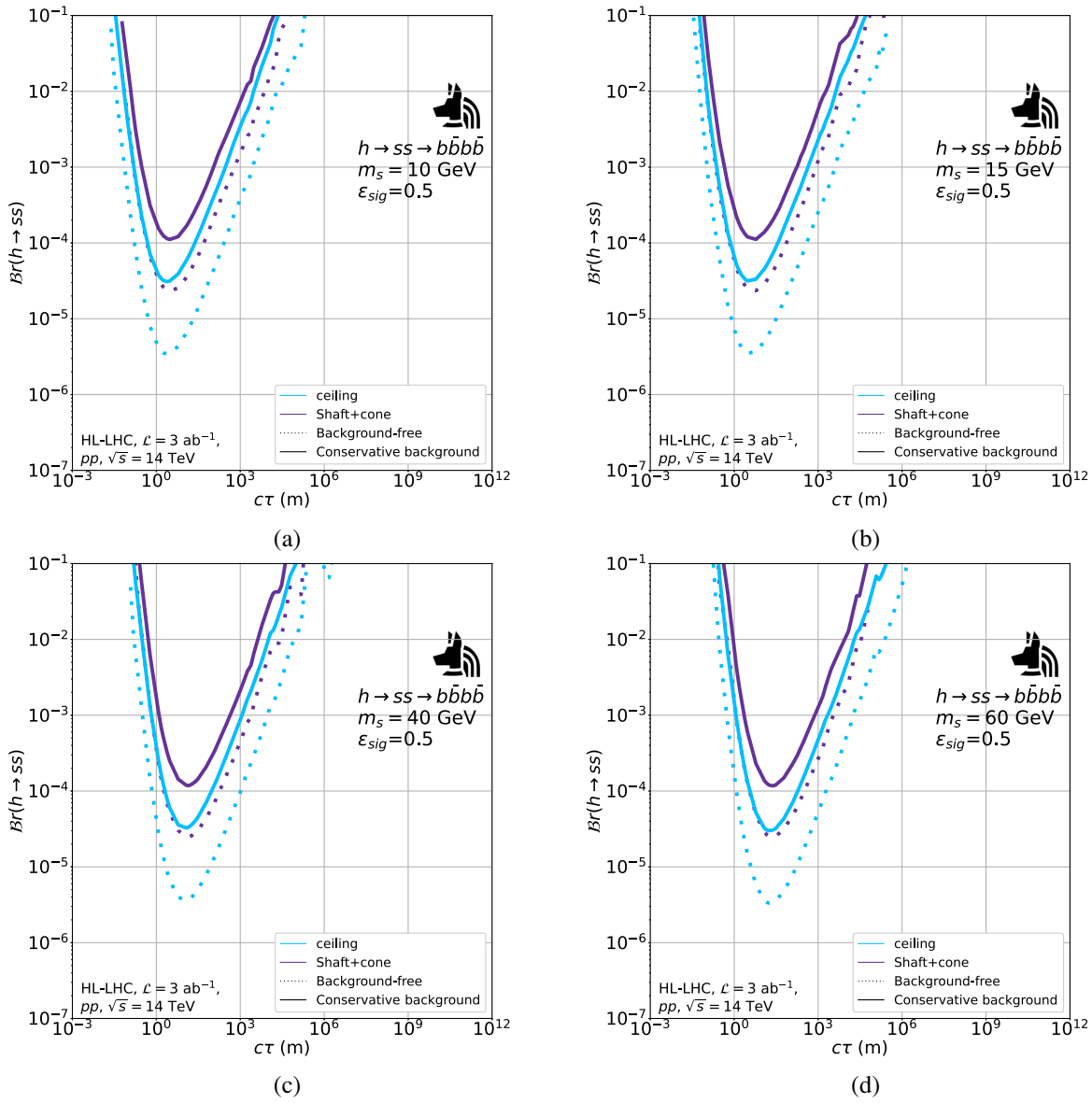


FIG. 11. 95% CL exclusion sensitivity of ANUBIS to an exotic branching ratio of the 125 GeV Higgs boson into a pair of long-lived scalars s with masses of (a) 10 GeV, (b) 15 GeV, (c) 40 GeV, and (d) 60 GeV using 3 ab^{-1} of pp collisions at the HL-LHC, for the ceiling (blue) and shaft (purple) configurations of the ANUBIS detector, with the 1DV selection. The projections are shown for the conservative (solid lines) and background-free (dotted lines) scenarios, which bracket the expected sensitivity of ANUBIS.

these collaborations exist for this signature. The projected HL-LHC exclusion limits at 95% CL from searches for Higgs boson decays into invisible particles $h \to$ invisible [65] are also shown for reference. The ANUBIS sensitivity is represented as a band where the lower (upper) edge corresponds to the background-free (conservative background) scenario. This highlights the range of potential branching ratios that could be probed between the best-case scenario and the expected conservative background level.

At its peak sensitivity at $c\tau \approx 12$ m, ANUBIS demonstrates an improvement in exclusion sensitivity of an exotic $\mathcal{B}r(h \to ss)$ by two to three orders of magnitude compared to the latest ATLAS and CMS results. Moreover, for $\mathcal{B}r(h \to ss) = 10^{-3}$, ANUBIS extends the $c\tau$ reach of ATLAS and CMS by three (four) orders of magnitude considering the conservative (background-free) projections, and can uniquely probe $c\tau$ values up to 10^3 m (10^4 m). Considering $\mathcal{B}r(h \to ss) = 10^{-2}$, ANUBIS' s $c\tau$ reach of 10^4 m (10^5 m) for conservative (background-free) projections approaches within three (two) orders of magnitude the limit set by Big Bang nucleosynthesis constraints [12]. Compared to ATLAS and CMS sensitivity projections at the HL-LHC discussed within the PBC group [66], ANUBIS provides one (two) orders of magnitude improvement in

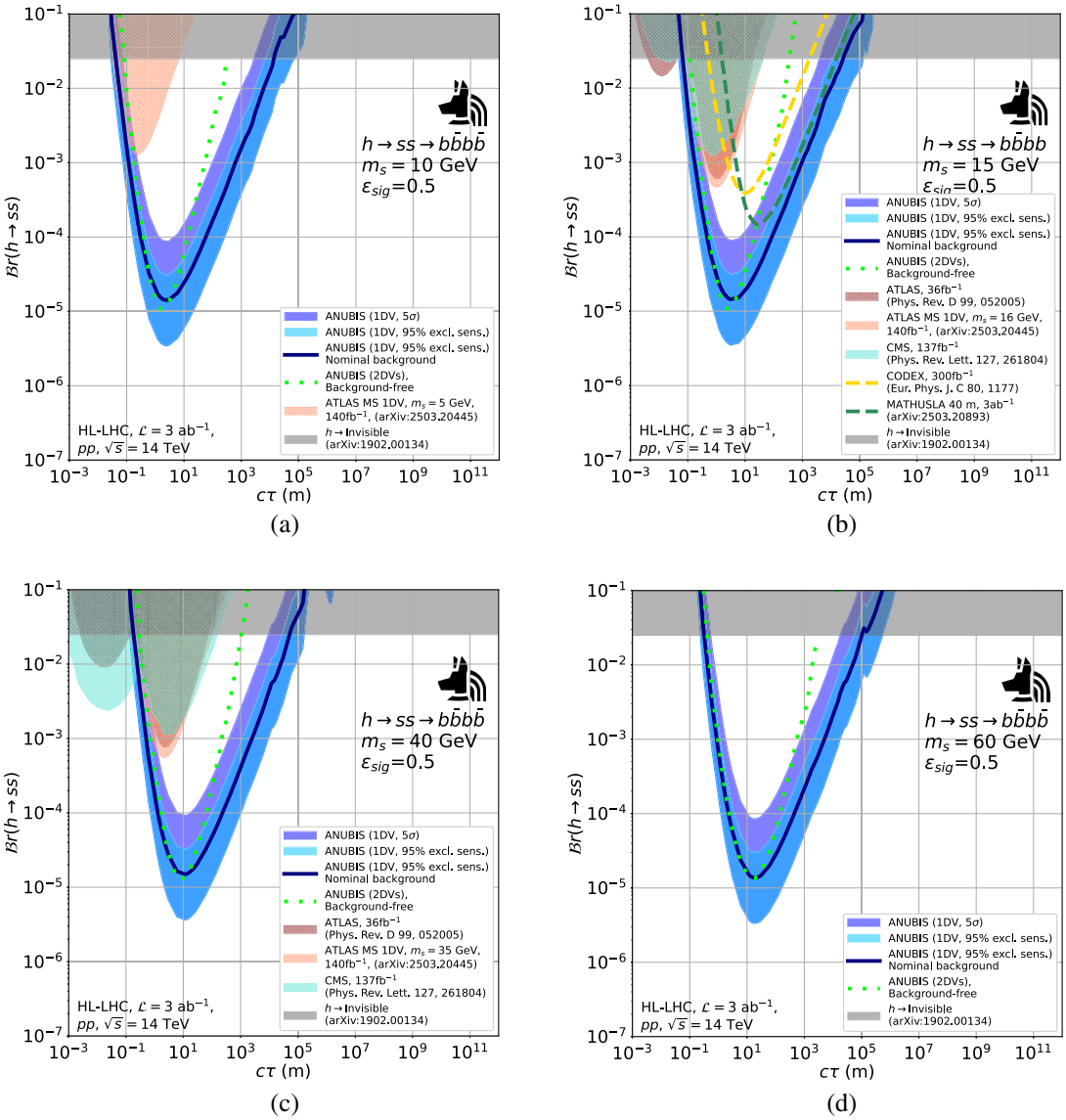


FIG. 12. Sensitivity of ANUBIS to an exotic branching ratio of the 125 GeV Higgs boson into a pair of long-lived scalars s with masses of (a) 10 GeV, (b) 15 GeV, (c) 40 GeV, and (d) 60 GeV using 3 ab^{-1} of pp collisions at the HL-LHC. The ANUBIS projections are shown as a band, where the lower (upper) edge corresponds to the background-free (conservative background) scenario for the 1DV selection. The nominal background scenario for the 1DV selection is shown as a solid line. The 5σ discovery and 95% CL exclusion limits are both shown, where they have a common lower edge. The background-free ANUBIS projection for the 2DVs selection is shown as a dotted line. For comparison, the sensitivity projections from other proposed transverse detectors CODEX-b [63], and MATHUSLA 40 m [64] at the HL-LHC are also presented, alongside the projected sensitivity from $h \to$ invisible decays at the HL-LHC [65]. The latest LHC results from ATLAS [20,41] and CMS [19] are also shown for reference.

sensitivity to an exotic $\mathcal{B}r(h \to ss)$ at $c\tau = 10^3$ m, and extends the $c\tau$ reach by more than one (two) orders of magnitude for conservative (background-free) projections.

Comparing the transverse experiments for the HL-LHC phase, both CODEX-b and ANUBIS reach their maximum sensitivity at $c\tau \approx 10$ m. Considering conservative (background-free) projections, ANUBIS surpasses CODEX-b by about one (two) orders of magnitude in terms of sensitivity to $\mathcal{B}r(h \to ss)$ across the entire $c\tau$ range for $m_s = 15$ GeV. Similarly, ANUBIS's conservative limits surpass the MATHUSLA 40 m projections for $c\tau \lesssim 50$ m for $m_s = 15$ by up to an order of magnitude, and ANUBIS's background-free projections surpass them across the whole $c\tau$ range and by up to three orders of magnitude for $c\tau \approx 5$ m.

In terms of the $c\tau$ reach and taking $\mathcal{B}r(h \to ss) = 10^{-3}$ as a benchmark, ANUBIS surpasses CODEX-b by two (three) orders of magnitude and MATHUSLA 40 m by one (two) orders of magnitude for conservative (background-free) projections for $m_s = 15$ GeV. Note that ANUBIS has the unique advantage among the transverse experiments,

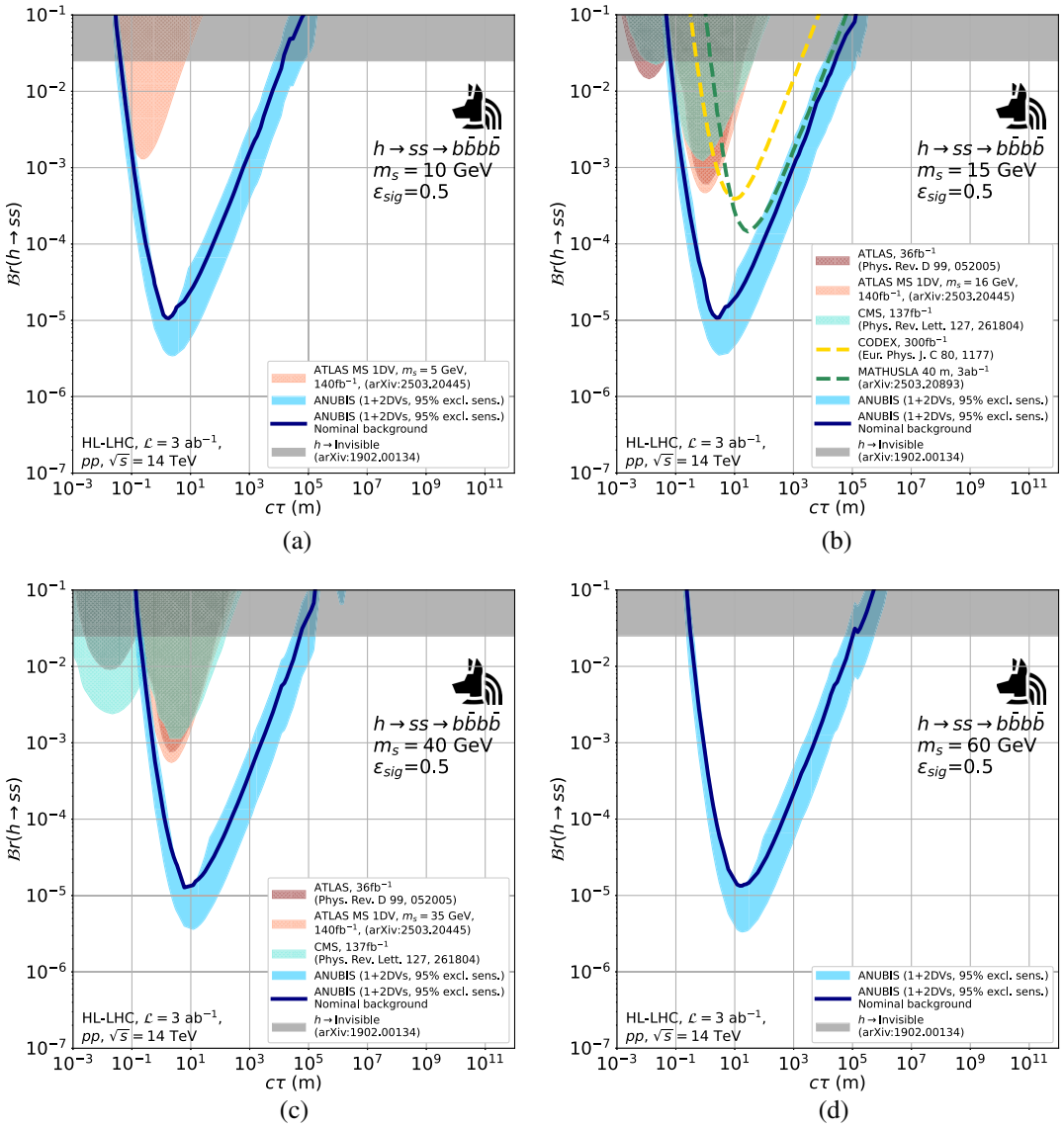


FIG. 13. 95% CL exclusion sensitivity of ANUBIS to an exotic branching ratio of the 125 GeV Higgs boson into a pair of long-lived scalars s with masses of (a) 10 GeV, (b) 15 GeV, (c) 40 GeV, and (d) 60 GeV using 3 ab^{-1} of pp collisions at the HL-LHC. The combined single and two displaced vertices projections for ANUBIS are shown as a band, the lower (upper) edge being the minimum of the background-free (conservative) 1DV and the 2DVs limits. The nominal background scenario for the 1DV selection is shown as a solid line. For comparison, the sensitivity projections from other proposed transverse detectors CODEX-b [63], and MATHUSLA 40 m [64] at the HL-LHC are also presented, alongside the projected sensitivity from $h \to$ invisible decays at the HL-LHC [65]. The latest LHC results from ATLAS [20,41] and CMS [19] are also shown for reference.

featuring a continuous active decay volume that, in combination with ATLAS, extends all the way to the interaction point. This allows for seamless coverage across the entire $c\tau$ range.

These sensitivity limits can be further improved using the 2DVs selection, which is effectively background-free. The combination of the 1DV and 2DVs limits then represents the optimized reach that ANUBIS would have to this model. Figure 13 shows this band, with the lower (upper) edge being the minimum of the background-free (conservative) 1DV and the 2DVs limits. This improves the maximum sensitivity in the conservative background scenario by up to half an order of magnitude, and gives a narrower band below $c\tau = \mathcal{O}(10)$ m.

The comparisons in terms of the sensitivity to $\mathcal{B}r(h \to ss)$ are summarized in Table I for four representative benchmarks with $m_s = 15\,\text{GeV}$ $(c\tau = 3, 100\,\text{m})$ and $m_s = 40\,\text{GeV}$ $(c\tau = 10, 100\,\text{m})$. The $c\tau$ reach for $\mathcal{B}r(h \to ss) = 10^{-3}$ is shown in Table II for $m_s = 15$ and 40 GeV. In combination with Fig. 12, both tables indicate that transverse experiments are an indispensable component of the experimental landscape of LLP searches at the HL-LHC,

TABLE I. The exclusion sensitivity of ANUBIS in the default ceiling configuration to $\mathcal{B}r(h \to ss)$ for $m_s = 15\,\text{GeV}$ with $c\tau = 3$ and 100 m, and $m_s = 40\,\text{GeV}$ with $c\tau = 10$ and 100 m, using 3 ab^{-1} of pp collisions at the HL-LHC. Both conservative (conserv.) and background-free (bg.-free) projections are shown, which bracket the expected ANUBIS sensitivity. For comparison, the sensitivity projections from other proposed transverse detectors CODEX-b [63], MATHUSLA 200 m [27] and MATHUSLA 40 m [64] at the HL-LHC are also presented, alongside the latest LHC results from ATLAS [41] and CMS [19] using ~140 fb^{-1} of pp collisions.

m_s	15 GeV	15 GeV	40 GeV	40 GeV
$c\tau$	3 m	100 m	10 m	100 m
ATLAS, **140 fb^{-1}**	1.1×10^{-3}	1.8×10^{-1}	1.8×10^{-3}	3.4×10^{-2}
CMS, **137 fb^{-1}**	2.4×10^{-3}	6.3×10^{-2}	1.8×10^{-3}	1.5×10^{-2}
CODEX-b	8.0×10^{-4}	1.6×10^{-3}	…	…
MATHUSLA 40	3.7×10^{-3}	2.4×10^{-4}	…	…
ANUBIS 1DV CLs conserv.	3.2×10^{-5}	2.5×10^{-4}	3.3×10^{-5}	1.0×10^{-4}
ANUBIS 1DV CLs bg.-free	3.5×10^{-6}	2.8×10^{-5}	3.7×10^{-6}	1.2×10^{-5}
ANUBIS 2DVs CLs conserv.	9.8×10^{-5}	1.3×10^{-2}	1.2×10^{-4}	2.0×10^{-3}
ANUBIS 2DVs CLs bg.-free	1.1×10^{-5}	1.5×10^{-3}	1.3×10^{-5}	2.2×10^{-4}
ANUBIS 1 + 2DVs CLs conserv.	1.1×10^{-5}	2.5×10^{-4}	1.3×10^{-5}	1.0×10^{-4}
ANUBIS 1 + 2DVs CLs bg.-free	3.5×10^{-6}	2.8×10^{-5}	3.7×10^{-6}	1.2×10^{-5}

TABLE II. The expected $c\tau$ reach of ANUBIS in the default ceiling configuration to an $\mathcal{B}r(h \to ss) = 0.001$ for $m_s = 15$ and 40 GeV using 3 ab^{-1} of pp collisions at the HL-LHC. Both conservative (conserv.) and background-free (bg.-free) projections are shown, which bracket the expected ANUBIS sensitivity. For comparison, the reach of other proposed transverse detectors CODEX-b [63], and MATHUSLA 40 m [64] at the HL-LHC are also presented, alongside the latest LHC results from ATLAS [41] and CMS [19] using ~140 fb^{-1} of pp collisions.

	$m_s = 15$ GeV	$m_s = 40$ GeV
ATLAS, **140 fb^{-1}**	$[4.6 \times 10^{-1}, 2.7]$ m	$[1.3, 4.6]$ m
CMS, **137 fb^{-1}**	…	…
CODEX-b	$[2.5, 6.1 \times 10^{1}]$ m	…
MATHUSLA 40	$[4.8, 5.8 \times 10^{2}]$ m	…
ANUBIS 1DV CLs conserv.	$[2.4 \times 10^{-1}, 4.3 \times 10^{2}]$ m	$[6.7 \times 10^{-1}, 1.2 \times 10^{3}]$ m
ANUBIS 1DV CLs bg.-free	$[1.1 \times 10^{-1}, 4.0 \times 10^{3}]$ m	$[3.2 \times 10^{-1}, 9.3 \times 10^{3}]$ m
ANUBIS 2DVs CLs conserv.	$[5.5 \times 10^{-1}, 2.2 \times 10^{1}]$ m	$[1.6, 6.8 \times 10^{1}]$ m
ANUBIS 2DVs CLs bg.-free	$[2.7 \times 10^{-1}, 7.9 \times 10^{1}]$ m	$[7.0 \times 10^{-1}, 2.2 \times 10^{2}]$ m
ANUBIS 1 + 2DVs CLs conserv.	$[2.4 \times 10^{-1}, 4.3 \times 10^{2}]$ m	$[6.7 \times 10^{-1}, 1.2 \times 10^{3}]$ m
ANUBIS 1 + 2DVs CLs bg.-free	$[1.1 \times 10^{-1}, 4.0 \times 10^{3}]$ m	$[3.2 \times 10^{-1}, 9.3 \times 10^{3}]$ m

significantly extending the reach of existing experiments. Furthermore, the results underline that ANUBIS is a competitive contender among the transverse detector initiatives.

The signal model used to determine these sensitivity limits corresponds to the BC5 benchmark [34] proposed by the CERN PBC study group [67]. In BC5, the key parameter of interest is the mixing angle, θ, between the scalar LLP and the Higgs boson assuming a fixed $\mathcal{B}r(h \to ss)$. Hence, the above sensitivity projections can be translated into constraints on θ using the formalism from Ref. [56], where this quantity is denoted by θ_s. Additional mass points at $m_s = 20$, 25, 30, and 50 GeV were also considered. The $\sin\theta$ interpretation is done assuming the BC5 recommendation of $\mathcal{B}r(h \to ss) = 0.01$, and the associated limits are shown in Fig. 14(a) for the combined 1DV and 2DVs case. To better represent ANUBIS's reach, the limits are also evaluated for $\mathcal{B}r(h \to ss) = 10^{-3}$ in Fig. 14(b). Remarkably, despite the branching ratio being reduced by one order of magnitude, the reach in $\sin\theta$ remains within approximately half an order of magnitude.

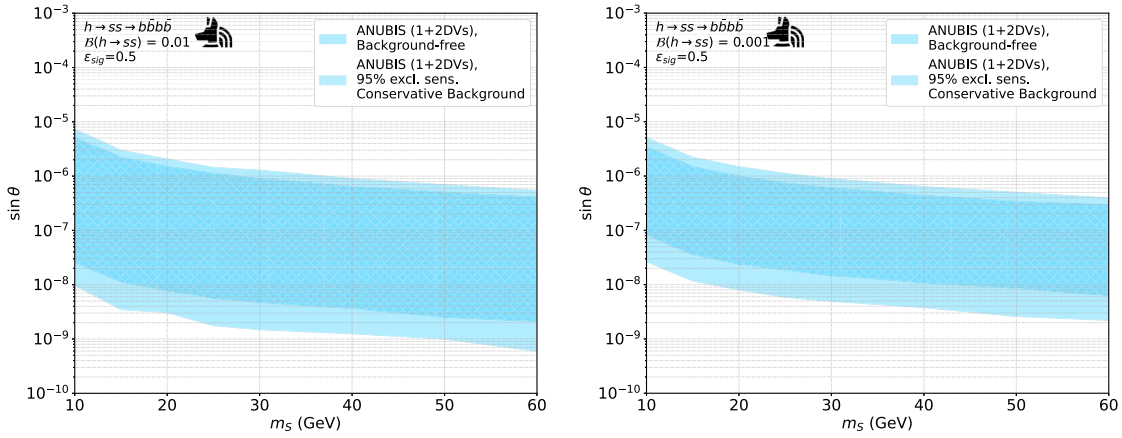


FIG. 14. Combined 1DV and 2DVs 95% CL exclusion $\sin\theta$ reach of ANUBIS in the ceiling configuration for $h \to ss$ decays using 3 ab^{-1} of pp collisions at the HL-LHC, where s are long-lived scalars decaying as $s \to b\bar{b}$, and θ is the mixing angle between the h and s scalars. For (a) BC5 benchmark with $\mathcal{B}r(h \to ss) = 10^{-2}$ [34], and (b) for $\mathcal{B}r(h \to ss) = 10^{-3}$. Both conservative (hatched area) and background-free (solid filled area) projections are shown, which bracket the expected ANUBIS sensitivity.

V. CONCLUSION AND OUTLOOK

In summary, the ANUBIS detector offers an unprecedented opportunity to dramatically extend the discovery potential of HL-LHC in the search for new physics beyond the SM through the detection of electrically neutral LLPs. This is achieved by instrumenting a large decay volume adjacent to the ATLAS experiment at the HL-LHC with tracking detectors. Due to its location transverse to the beamline and close to the ATLAS interaction point, ANUBIS will provide unique sensitivity to LLPs with decay lengths of $>\mathcal{O}(10\ \mathrm{m})$ produced at partonic center-of-mass energies $\sqrt{\hat{s}}$ corresponding to the electroweak scale and above. Hence, the ANUBIS detector will complement the discovery potential of the main HL-LHC detectors like ATLAS, CMS, and LHCb and forward/fixed target detectors like FASER/SHiP, which are limited in their decay length and $\sqrt{\hat{s}}$ reach, respectively, cf., Fig. 1.

The two proposed detector layouts for ANUBIS were outlined, their physics potential was assessed, and comparisons to other experiments were drawn. The ceiling configuration of the ANUBIS detector was identified as the preferred one, both in terms of practical considerations for the installation and HL-LHC/ATLAS operations, and in terms of the physics potential. The ceiling configuration is now the default for the ANUBIS detector. It foresees instrumenting the ceiling of the UX15 ATLAS experimental cavern and the bottom of the PX14 and PX16 service shaft with tracking stations using RPC detectors.

The potential sources of background were discussed, identifying hadronic interactions of K_L^0 and n with material as the dominant contribution, which can be strongly reduced using dedicated selections. This underlines the main advantage of the ANUBIS detector featuring a large air-filled decay volume between the ATLAS detector and the cavern ceiling, combined with the adjacency to the interaction point. The background contributions were estimated using a data-driven method. For the default ceiling configuration of the ANUBIS detector, an exclusion sensitivity at 95% CL was found, corresponding to at most 36 signal events. For a discovery sensitivity at 5σ CL, 102 of exotic LLPs events were found to be sufficient under conservative assumptions, leaving ample potential for further background reduction. The topology of potential background events was studied using MC simulations to guide future sensitivity optimizations.

The sensitivity of ANUBIS was evaluated in the context of the Benchmark Case 5 of the Physics Beyond Colliders initiative that features two scalar LLPs s produced in an exotic decay of the 125 GeV Higgs boson and decaying into $b\bar{b}$ quark pairs each. Overall, ANUBIS is expected to probe $\mathcal{B}r(h \to ss)$ down to 1.3×10^{-5}. This marks an improvement of over an order of magnitude beyond projected ATLAS and CMS capabilities at the HL-LHC, and surpasses other transverse experiment proposals CODEX-b and MATHUSLA. Assuming further sensitivity improvements beyond the conservative assumptions in the background estimate, a sensitivity to $\mathcal{B}r(h \to ss)$ of down to 3.3×10^{-6} could be achieved. For $\mathcal{B}r(h \to ss) = 0.001$, an unprecedented $c\tau$ range from $\mathcal{O}(0.1\ \mathrm{m})$ to $\mathcal{O}(10^3\ \mathrm{m})$ could be probed according to conservative projections. This reach could be potentially extended up to $c\tau \approx 10^4$ m.

A. Outlook

Active R&D efforts aimed at the realization of the ANUBIS detector are underway. The aforementioned prototype demonstrator *pro*ANUBIS consisting of one ANUBIS tracking station module has recorded 177 fb^{-1} of pp collision data at $\sqrt{s} = 13.6$ TeV in 2024–2025 [31,32].

The analysis of *pro*ANUBIS data is ongoing, allowing to refine the tracking and vertexing algorithms, inform detector performance benchmarks [33], improve background simulations, and further geometry optimizations for ANUBIS. Furthermore, strong and concerted efforts are underway to systematically study alternative RPC gas mixtures within the context of the DRD1 Collaboration [68–70]. The goal is adhering to EU regulations by achieving a global warming potential below 150 times that of CO_2 without compromising on detector performance. Several promising mixtures that are expected to perform well in the moderate rate environment $\gtrsim$20 m away from the ATLAS IP have been identified. In parallel, efforts are underway to assess and ensure the mechanical integrity of RPC gas gaps to prevent any gas leaks at the source. A novel methodology for accelerated ageing of RPC gas gaps using thermal cycling has been established in the context of the Phase II upgrade of the ATLAS RPCs, informing the redesign of their gas gaps [71].

Beyond this work, concerted efforts are underway to map out the sensitivity of the ANUBIS detector to alternative LLP scenarios. To facilitate these studies, a user-friendly modular framework SET-ANUBIS has been developed. The primary focus is to map out the sensitivity to PBC benchmark models. For example, the sensitivity to heavy neutral leptons (HNLs) that couple exclusively to first or second generation leptons, i.e., PBC Benchmark Cases 6 and 7, has been published recently [72]. Beyond PBC benchmarks, other scenarios where ANUBIS + ATLAS are expected to provide unprecedented sensitivity such as photophobic axionlike particles produced in association with W or Z bosons are being actively explored.

ACKNOWLEDGMENTS

Particular thanks go to: Ben Allanach, Cristiano Alpigiani, David Curtin, Albert De Roeck, Miriam Diamond, Erez Etzion, Simon Knapen, Gaurav Kumar, Steven Lowette, Maxim Ovchinnikov, Runze Ren, Heather Russell, Richard Shaw, and Gustavo Uribe. The authors would like to express their gratitude to: the ATLAS Collaboration for hosting *pro*ANUBIS, facilitating the data taking and data analysis, and provision of consumables; the ATLAS RPC community for their guidance with constructing the RPCs for *pro*ANUBIS and the chamber cages, and maintenance/troubleshooting; and the ATLAS Technical Coordination team for help with installing, connection of services, maintenance, and safety; to the colleagues in the CODEX-b collaboration for lending front-end board electronics to allow for a timely installation of the *pro*ANUBIS demonstrator; to the PBC BSM group and especially group conveners Felix Kahlhoefer and Torben Ferber for their guidance and efficient moderation of the scientific discussions, and finally, to colleagues in the wider LLP community for the scrutiny of our results and thoughtful suggestions. We gratefully acknowledge the support of UKRI under the Future Leaders Fellowship scheme.

DATA AVAILABILITY

The data that support the findings of this article are not publicly available. The data are available from the authors upon reasonable request.

[1] R. Barbier *et al.*, R-parity violating supersymmetry, Phys. Rep. **420**, 1 (2005).
[2] G. F. Giudice and R. Rattazzi, Theories with gauge mediated supersymmetry breaking, Phys. Rep. **322**, 419 (1999).
[3] T. Han, Z. Si, K. M. Zurek, and M. J. Strassler, Phenomenology of hidden valleys at hadron colliders, J. High Energy Phys. 07 (2008) 008.
[4] M. J. Strassler and K. M. Zurek, Echoes of a hidden valley at hadron colliders, Phys. Lett. B **651**, 374 (2007).
[5] Z. Chacko, H.-S. Goh, and R. Harnik, The twin Higgs: Natural electroweak breaking from mirror symmetry, Phys. Rev. Lett. **96**, 231802 (2006).
[6] H. Cai, H.-C. Cheng, and J. Terning, A quirky little Higgs model, J. High Energy Phys. 05 (2009) 045.
[7] G. Burdman, Z. Chacko, H.-S. Goh, and R. Harnik, Folded supersymmetry and the LEP paradox, J. High Energy Phys. 02 (2007) 009.
[8] L. J. Hall, J. March-Russell, and S. M. West, A unified theory of matter genesis: Asymmetric freeze-in, arXiv:1010.0245.
[9] C. Cheung, G. Elor, L. J. Hall, and P. Kumar, Origins of hidden sector dark matter II: Collider physics, J. High Energy Phys. 03 (2011) 085.
[10] K. M. Zurek, Asymmetric dark matter: Theories, signatures, and constraints, Phys. Rep. **537**, 91 (2014).
[11] K. Barry, P. W. Graham, and S. Rajendran, Displaced vertices from R -parity violation and baryogenesis, Phys. Rev. D **89**, 054003 (2014).
[12] A. Fradette and M. Pospelov, BBN for the LHC: Constraints on lifetimes of the Higgs portal scalars, Phys. Rev. D **96**, 075033 (2017).
[13] L. R. Evans and P. Bryant, LHC machine, J. Instrum. **3**, S08001 (2008), This report is an abridged version of the LHC Design Report, CERN Report No. CERN-2004-003.
[14] ATLAS Collaboration, The ATLAS experiment at the CERN large hadron collider, J. Instrum. **3**, S08003 (2008), Also published by CERN Geneva in 2010.
[15] CMS Collaboration, The CMS experiment at the CERN LHC. The Compact Muon Solenoid experiment, J. Instrum.

3, S08004 (2008), Also published by CERN Geneva in 2010.
[16] LHCb Collaboration, The LHCb detector at the LHC, J. Instrum. **3**, S08005 (2008).
[17] J. Alimena *et al.*, Searching for long-lived particles beyond the standard model at the large hadron collider, J. Phys. G **47**, 090501 (2020).
[18] CMS Collaboration, Search for long-lived particles decaying into muon pairs in proton-proton collisions at $\sqrt{s} = 13$ TeV collected with a dedicated high-rate data stream, J. High Energy Phys. 04 (2022) 062.
[19] CMS Collaboration, Search for long-lived particles decaying in the CMS end cap muon detectors in proton-proton collisions at $\sqrt{s} = 13$ TeV, Phys. Rev. Lett. **127**, 261804 (2021).
[20] ATLAS Collaboration, Search for long-lived particles produced in pp collisions at $\sqrt{s} = 13$ TeV that decay into displaced hadronic jets in the ATLAS muon spectrometer, Phys. Rev. D **99**, 052005 (2019).
[21] R. Alemany Fernández *et al.* (PBC Collaboration), Summary report of the Physics Beyond Colliders study at CERN, arXiv:2505.00947.
[22] C. Antel *et al.*, Feebly-interacting particles: FIPs 2022 Workshop Report, Eur. Phys. J. C **83**, 1122 (2023).
[23] C. Ahdida *et al.* (SHiP Collaboration), SHiP Experiment—Progress Report, Technical Reports No. CERNSPSC-2019-010, No. SPSC-SR-248, CERN, Geneva, 2019, https://cds.cern.ch/record/2654870.
[24] M. Bauer, O. Brandt, L. Lee, and C. Ohm, ANUBIS: Proposal to search for long-lived neutral particles in CERN service shafts, arXiv:1909.13022, 10.1103/n652-fgyb, accepted by APS Open Sci.
[25] V. V. Gligorov, S. Knapen, B. Nachman, M. Papucci, and D. J. Robinson, Leveraging the ALICE/L3 cavern for long-lived particle searches, Phys. Rev. D **99**, 015023 (2019).
[26] V. V. Gligorov, S. Knapen, M. Papucci, and D. J. Robinson, Searching for long-lived particles: A compact detector for exotics at LHCb, Phys. Rev. D **97**, 015023 (2018).
[27] J. P. Chou, D. Curtin, and H. J. Lubatti, New detectors to explore the lifetime frontier, Phys. Lett. B **767**, 29 (2017).
[28] D. Curtin *et al.*, Long-lived particles at the energy frontier: The MATHUSLA physics case, Rep. Prog. Phys. **82**, 116201 (2019).
[29] MATHUSLA Collaboration, An update to the letter of intent for MATHUSLA: Search for long-lived particles at the HL-LHC, arXiv:2009.01693.
[30] A. Shah for the ANUBIS Collaboration, Searches for long-lived particles with the ANUBIS experiment, Proc. Sci. EPS-HEP2023 (**2024**) 051. [arXiv:2401.11604].
[31] ANUBIS Collaboration, Construction of proANUBIS: A proof-of-concept detector for the ANUBIS experiment, Nucl. Instrum. Methods Phys. Res., Sect. A **1091**, 171687 (2026).
[32] ANUBIS Collaboration, Commissioning of proANUBIS: A proof-of-concept detector for the ANUBIS experiment, Nucl. Instrum. Methods Phys. Res., Sect. A **1089**, 171501 (2026).
[33] ANUBIS Collaboration, Calibration and performance of proANUBIS: A proof-of-concept detector for the ANUBIS experiment, arXiv:2606.26856.
[34] J. Beacham *et al.*, Physics Beyond Colliders at CERN: Beyond the standard model working group report, J. Phys. G **47**, 010501 (2020).
[35] L. Pontecorvo *et al.* (private communication).
[36] D. Sankey (private communication).
[37] ATLAS Collaboration, ATLAS muon spectrometer: Technical design report, CERN Reports No. CERN-LHCC-97-22, No. ATLAS-TDR-10, 1997, https://cds.cern.ch/record/331068.
[38] V. Brdar, A. J. Helmboldt, S. Iwamoto, and K. Schmitz, Type I seesaw mechanism as the common origin of neutrino mass, baryon asymmetry, and the electroweak scale, Phys. Rev. D **100**, 075029 (2019).
[39] K. Bondarenko, A. Boyarsky, D. Gorbunov, and O. Ruchayskiy, Phenomenology of GeV-scale heavy neutral leptons, J. High Energy Phys. 11 (2018) 032.
[40] D. Gorbunov and M. Shaposhnikov, How to find neutral leptons of the νMSM?, J. High Energy Phys. 10 (2007) 015; 11 (2013) 101(E).
[41] ATLAS Collaboration, Search for events with one displaced vertex from long-lived neutral particles decaying into hadronic jets in the ATLAS muon spectrometer in pp collisions at $\sqrt{s} = 13$ TeV, Phys. Rev. D **112**, 092001 (2025).
[42] M. Bauer, M. Neubert, and A. Thamm, Collider probes of axion-like particles, J. High Energy Phys. 12 (2017) 044.
[43] S. Navas *et al.* (Particle Data Group), Review of particle physics, Phys. Rev. D **110**, 030001 (2024).
[44] TOTEM Collaboration, First measurement of elastic, inelastic and total cross-section at $\sqrt{s} = 13$ TeV by TOTEM and overview of cross-section data at LHC energies, Eur. Phys. J. C **79**, 103 (2019).
[45] ATLAS Collaboration, Measurement of the inelastic proton-proton cross section at $\sqrt{s} = 13$ TeV with the ATLAS detector at the LHC, Phys. Rev. Lett. **117**, 182002 (2016).
[46] LHCb Collaboration, Measurement of the inelastic pp cross-section at a centre-of-mass energy of 13 TeV, J. High Energy Phys. 06 (2018) 100.
[47] ATLAS Collaboration, Standalone vertex finding in the ATLAS muon spectrometer, J. Instrum. **9**, P02001 (2014).
[48] ATLAS Collaboration, Interactive web pages for radiation environment exploration of ATLAS, CERN Report No. ATL-SOFT-PUB-2020-003, 2020, https://cds.cern.ch/record/2742378.
[49] T. P. Satterthwaite, Sensitivity of the ANUBIS and ATLAS detectors to neutral long-lived particles produced in pp collisions at the large hadron collider, MPhil thesis, University of Cambridge, 2022, Report No. CERN-THESIS-2022–169.
[50] T. Sjöstrand, S. Ask, J. R. Christiansen, R. Corke, N. Desai, P. Ilten, S. Mrenna, S. Prestel, C. O. Rasmussen, and P. Z. Skands, An introduction to PYTHIA 8.2, Comput. Phys. Commun. **191**, 159 (2015).
[51] A. D. Martin, W. J. Stirling, R. S. Thorne, and G. Watt, Parton distributions for the LHC, Eur. Phys. J. C **63**, 189 (2009).

[52] ATLAS Collaboration, Summary of ATLAS Pythia 8 tunes, CERN Report No. ATL-PHYS-PUB-2012-003, 2012, https://cds.cern.ch/record/1474107.
[53] S. Agostinelli *et al.* (GEANT4 Collaboration), Geant4–a simulation toolkit, Nucl. Instrum. Methods Phys. Res., Sect. A **506**, 250 (2003).
[54] *High-Luminosity Large Hadron Collider (HL-LHC): Preliminary Design Report*, edited by G. Apollinari, I. Béjar Alonso, O. Brüning, M. Lamont, and L. Rossi (2015), 10.5170/CERN- 2015-005.
[55] S. Argyropoulos, O. Brandt, and U. Haisch, Collider searches for dark matter through the Higgs lens, Symmetry **13**, 2406 (2021).
[56] D. Curtin *et al.*, Exotic decays of the 125 GeV Higgs boson, Phys. Rev. D **90**, 075004 (2014).
[57] D. Curtin, R. Essig, S. Gori, and J. Shelton, Illuminating dark photons with high-energy colliders, J. High Energy Phys. 02 (2015) 157.
[58] J. Alwall, R. Frederix, S. Frixione, V. Hirschi, F. Maltoni, O. Mattelaer, H.-S. Shao, T. Stelzer, P. Torrielli, and M. Zaro, The automated computation of tree-level and next-to-leading order differential cross sections, and their matching to parton shower simulations, J. High Energy Phys. 07 (2014) 079.
[59] R. D. Ball *et al.* (NNPDF Collaboration), Parton distributions with QED corrections, Nucl. Phys. **B877**, 290 (2013).
[60] O. Brandt and P. Swallow for the ANUBIS Collaboration, 2026 ESPPU input from the ANUBIS Collaboration, arXiv:2504.03195.
[61] G. Cowan, Discovery sensitivity for a counting experiment with background uncertainty, Last Accessed Sep 2025, 2012, https://www.pp.rhul.ac.uk/~cowan/stat/medsig/medsigNote.pdf.
[62] A. L. Read, Presentation of search results: The CL_s technique, J. Phys. G **28**, 2693 (2002).
[63] CODEX-b Collaboration, Expression of interest for the CODEX-b detector, Eur. Phys. J. C **80**, 1177 (2020).
[64] MATHUSLA Collaboration, Conceptual design report for the MATHUSLA long-lived particle detector near CMS, arXiv:2503.20893.
[65] M. Cepeda *et al.*, Report from working group 2: Higgs physics at the HL-LHC and HE-LHC, CERN Yellow Rep. Monogr. **7**, 221 (2019).
[66] D. Curtin, Presentation at the BSM group meeting of the Physics Beyond Colliders initiative on 20/05/2025, 2025.
[67] R. Alemany *et al.*, Summary report of Physics Beyond Colliders at CERN, arXiv:1902.00260.
[68] A. Shah, T. Adolphus, Y. Zhang, and O. Brandt, Performance studies of thin gas gap resistive plate chamber prototypes with low global warming potential gases for the ANUBIS experiment, Nucl. Instrum. Methods Phys. Res., Sect. A **1080**, 170711 (2025).
[69] D. Ahmadi *et al.*, Performance and long-term aging studies on eco-friendly resistive plate chamber detectors, J. Instrum. **21**, C02004 (2026).
[70] RPC EcoGas@GIF++ Collaboration, Performance and long-term aging studies on eco-friendly resistive plate chamber detectors, Nucl. Instrum. Methods Phys. Res., Sect. A **1080**, 170624 (2025).
[71] A. Shah, Quality assurance tests and techniques to investigate and improve hermeticity of ATLAS Phase II resistive plate chamber detectors, Nucl. Instrum. Methods Phys. Res., Sect. A **1076**, 170510 (2025).
[72] M. Bauer, R. Bentham, O. Brandt, S. N. Erner, A. Mullin, D. Peng, T. Reymermier, and P. Swallow (ANUBIS), Projected sensitivity of the ANUBIS detector to heavy neutral leptons, arXiv:2606.26862.